Published in final edited form as:

Nature. 2021 August ; 596(7870): 97–102. doi:10.1038/s41586-021-03756-0.

Gut cytokines modulate olfaction through metabolic reprogramming of glia

Xiaoyu Tracy Cai[1,2,3], **Hongjie Li**[4,5,6], **Martin Borch Jensen**[2,7], **Elie Maksoud**[2], **Jovencio Borneo**[8], **Yuxin Liang**[9], **Stephen R. Quake**[10,11], **Liqun Luo**[4], **Pejmun Haghighi**[2], **Heinrich Jasper**[1,2,*]

[1]Immunology Discovery, Genentech, Inc., 1 DNA Way, South San Francisco, CA 94080, USA.

[2]Buck Institute for Research on Aging, 8001 Redwood Boulevard, Novato, CA 94945-1400, USA.

[3]University of Southern California, Los Angeles, CA 90007, USA.

[4]Department of Biology and Howard Hughes Medical Institute, Stanford University, Stanford, CA 94305, USA

[5]Huffington Center on Aging, Baylor College of Medicine, Houston, TX 77030, USA

[6]Department of Molecular and Human Genetics, Baylor College of Medicine, Houston, TX 77030, USA

[7]Gordian Biotechnology, 953 Indiana St., San Francisco, CA 94107, USA.

[8]FACS lab, Genentech, Inc., 1 DNA Way, South San Francisco, CA 94080, USA.

[9]NGS lab, Genentech, Inc., 1 DNA Way, South San Francisco, CA 94080, USA.

[10]Department of Bioengineering and Department of Applied Physics, Stanford University, Stanford, CA 94305, USA

[11]Chan Zuckerberg Biohub, Stanford, CA 94305, USA

Abstract

Infection-induced aversion against enteropathogens is a conserved sickness behavior that can promote host survival[1,2]. The etiology of this behavior remains poorly understood, but studies in *Drosophila* have linked olfactory and gustatory perception to avoidance behaviors against toxic microbes[3–5]. Whether and how enteric infections directly influence sensory perception to induce or modulate such behaviors remains unknown. Here we show that enteropathogen infection in *Drosophila* can modulate olfaction through metabolic reprogramming of ensheathing

[*]**Corresponding author:** Heinrich Jasper, Genentech, 1 DNA Way, South San Francisco, California 94080, USA. jasperh@gene.com.

Author contributions

X.T.C. and H.J. designed all experiments. H.L. performed scRNA-seq experiments and analysis. L.L. and S.R.Q. provided resources and guidance for scRNA-seq experiments. M.B.J, E.M. and P.H. contributed ideas and experiments to Fig.1g and Extended Data Fig.4a–4d. J.B. contributed to glia sorting in Extended Data Fig.7g. Y.L. performed Bulk RNA sequencing in Extended Data Fig.7. X.T.C. performed all other experiments and analyzed the data. X.T.C. and H.J. wrote the manuscript with input from the other authors.

Competing interests

X.T.C., is an employee of Genentech Inc., a Roche subsidiary.

H.J., J.B., and Y.L. are employees and shareholders of Genentech Inc., a Roche subsidiary.

M.B.J. is employee and shareholder of Gordian Biotechnology.

glia (EG) of the antennal lobe (AL). Infection-induced Unpaired cytokine expression in the intestine activates JAK/STAT signaling in EG, inducing the expression of glial monocarboxylate transporters (MCTs) and the apolipoprotein *glial lazarillo* (*Glaz*), and thus impacting glia/neuron metabolic coupling in the AL. This modulates olfactory discrimination, promoting avoidance of bacteria-laced food and increasing animal survival. While transient in young animals, gut-induced metabolic reprogramming of EG becomes constitutive in old animals due to age-related intestinal inflammation, contributing to an age-related decline in olfactory discrimination. Our findings identify adaptive glial metabolic reprogramming by gut-derived cytokines as a mechanism causing lasting changes in a sensory system in the aging animal.

Introduction

Olfactory perception influences nutrition and promotes physiological and mental well-being[6,7]. In flies, a dedicated olfactory circuit elicits avoidance behaviors towards Geosmin, a volatile compound released by mold and some bacteria[4]. Olfactory receptors also mediate an initial attraction to food containing certain enteropathogens[3,5]. After infection with these pathogens, however, an avoidance behavior is triggered by immune receptors in the brain[3], gustatory bitter neurons, and the neuropeptide Leukokinin[5]. Whether changes in olfactory perception contribute to this behavioral switch from attraction to avoidance remains unclear.

In *Drosophila*, odorants are sensed by olfactory receptor neurons (ORNs) in the head, the antenna and the maxillary palp. ORNs synapse into projection neurons (PNs) at the antennal lobe (AL), where the signal is converted into a spatiotemporal code in 50 glomerular compartments[8]. PN axons project to higher olfactory centers to instruct innate and learned behavior. In this system, glia and neurons operate as a tightly coupled unit to maintain olfactory sensitivity[9,10].

In aging flies, olfactory perception of both aversive and attractive odors declines[11], but the mechanism(s) of this decline remain unclear. Olfactory perception and other neurological processes also decline in aging mammals, often influenced by gastrointestinal signals,[12,13].

Here, we investigate the communication between the gut and the brain, and how it influences infection-induced avoidance behavior, infection tolerance, as well as olfactory decline during aging.

Results

Enteric infection modulates olfaction

We used a modified CAFE assay to measure choice between food containing or not *Erwinia Carotovora Carotovora 15* (*Ecc15*), a non-lethal enteropathogen that causes intestinal inflammation[14] (Extended Data Fig.1a). Consistent with recent reports[3], naïve flies consumed more *Ecc15*-containing food than normal food (Fig.1a). But when orally infected with *Ecc15* for 24 hours prior to the feeding assay, flies developed a distinct aversion to food containing *Ecc15* (Fig.1a, Extended Data Fig.1b). To assess whether this involved changes in olfactory perception, we determined the “preference index” (P.I.) for attractive (such as Putrescine[11]) or aversive odors (such as 3-Octanol[11]) in T-maze assays[11] (Extended Data

Fig.1c). Preference or aversion for attractive or aversive odors, respectively, declined upon infection, indicating that infection causes a non-selective decline in olfactory discrimination (Fig.1b, Extended Data Fig.1d). This was transient, as 5 days after infection, olfactory discrimination recovered (Fig.1b, Extended Data Fig.1d), coincident with clearance of bacteria and epithelial regeneration in the intestine[15]. Olfactory discrimination was not influenced by starvation or by exposure to heat-killed *Ecc15* (Extended Data Fig.1e, 1f). Consistent with their reported role in sensing pathogenic bacteria[3,5], the CO2 receptor Gr63a or the odorant receptor coreceptor Orco were required for the attraction to *Ecc15* food: *Orco*^{1} and *Gr63a*^{1} mutants ingested less *Ecc15* food under naïve conditions, and when infected, failed to further reduce ingestion of *Ecc15* containing food (Extended Data Fig.1g). Together, these observations suggest that after an initial odorant-mediated attraction, flies develop aversion to enteropathogens, through a concerted activation of gustatory and immune receptors[3,5] and suppression of olfaction.

Upon oral infection with *Ecc15*, damaged intestinal enterocytes (ECs) produce the inflammatory IL6-like cytokines, Unpaired 2 and 3 (Upd2 and Upd3), to stimulate intestinal stem cell (ISC) proliferation and epithelial regeneration[14]. Upds activate the JAK/STAT signaling pathway through the receptor Domeless (Dome) and the JAK homologue Hopscotch (Hop). Using 2xSTAT::GFP, a reporter for JAK/STAT pathway activity[16], we found upregulated GFP expression in the brain 4 hours post oral *Ecc15* infection, as well as after oral infection with *Pseudomonas Entomophila (PE)*, a more lethal enteropathogen that damages the gut epithelium[15] (Fig.1c, Extended Data Fig.1h). JAK/STAT activity was observed in a sparse population of cells of the brain that stained positive for the glial marker Repo (Extended Data Fig.1i). Subtype-specific Gal4 drivers revealed that among the five subtypes of *Drosophila* glia (astrocytes, ensheathing, perineural, subperineural, and cortex glia[17]), ensheathing glia (EG) were the main population upregulating STAT activity in response to *Ecc15* infection (Fig.1d, Extended Data Fig.2a). This was confirmed using four different Gal4 drivers to label EG (Extended Data Fig.2b–2d) and by flow cytometry (Extended Data Fig.2e). Infection did not influence numbers (Extended Data Fig.2c) and membranous processes (labeled using UAS::mCD4GFP) of EG at the AL (Extended Data Fig.2f), and glomerular compartmentalization in the AL and lobe size remained unaffected (Extended Data Fig.2f). JAK/STAT activation in EG was sufficient and required for infection-induced changes in olfactory discrimination, as over-expressing constitutively active Hop (*Hop*^{tuml}) in EG reduced olfactory discrimination (Fig.1e), while loss of Dome or STAT in all glia (repo::Gal4), or specifically in EG (GMR56F03::Gal4), rescued the decline of olfactory discrimination caused by *Ecc15* infection (Fig.1e, Extended Data Fig.3a, 3b). Over-expression of *Hop*^{tuml} in EG also reduced ingestion of *Ecc15*-containing food and promoted survival of flies fed *PE* containing food, while Dome or STAT knockdown in EG increased ingestion of *Ecc15*-containing food in infected flies and increased mortality on *PE* containing food (Fig.1f, Extended Data Fig.3d–3h). We propose that the corresponding changes in ingestion of *PE*-laced food contribute to reduced mortality, but it is possible that additional genetic background conditions influence mortality, as seen for example in *Orco* mutant flies, which ingest less bacteria (Extended Data Fig.1g) but show increased susceptibility to *PE* (Extended Data Fig.3i).

Gut-derived Upds regulate olfaction

To test whether gut-derived Upds directly contribute to the infection-induced activation of JAK/STAT signaling in EGs, we used intestinal enterocyte (EC)-specific perturbations using Mex1::Gal4, an EC driver with no expression in the brain (Extended Data Fig.4a, 4b). Indeed, JAK/STAT activation in glia at the AL could be triggered in naïve flies or prevented in infected flies by over-expression or knockdown, respectively, of Upd2 and Upd3 in ECs (Fig.1g, Extended Data Fig.4c, 4d). Consistently, EC-derived Upd2 and Upd3 were sufficient and required for the modulation of olfactory discrimination caused by infection (Fig.1h, Extended Data Fig.4e–4g). Knockdown of Upd2 or Upd3 did not affect olfaction in naïve flies (Extended Data Fig.4f), and perturbing these ligands in fatbody (cg::Gal4) or hemocytes (hml::Gal4), tissues that are sources for Upds in other contexts[18,19], did not significantly impact STAT activity in glia at the AL (Extended Data Fig.4h–4k).

Chronic JAK activation impairs aging EG

Loss of olfactory sensitivity is an early sign of normal aging and neurodegeneration[20]. In aging *Drosophila*, olfactory perception was reported to deteriorate before vision[11], a decline that we were able to recapitulate in our T-maze assays (Fig.2a). Glomerular compartments in the AL became less organized and less distinct in geriatric (60–70 day old) animals (Extended Data Fig.5a) and AL size increased with age (Extended Data Fig.5b). This correlates with a reduction in the number of EG and of glial membranous processes (Extended Data Fig.5b), changes that are expected to impact AL structure[10], and thus likely contribute to the age-related decline in olfaction.

Aging in *Drosophila* is accompanied by the development of intestinal inflammation, and is associated with the constitutive expression and release of Upd cytokines[21]. Consistently, JAK/STAT activity in AL EG was elevated in old flies (Fig.2b, Extended Data Fig.5c), and knockdown of Dome or STAT in EG specifically (Fig.2c; Extended Data Fig.5d) or in all glia (Extended Data Fig.5d) rescued the decline of olfactory discrimination in old animals. Loss of Dome in EG also rescued the age-related decline of EGs and restored the size of the AL (Extended Data Fig.5e). JAK/STAT activation in EG of old animals is a consequence of intestinal Upd release, as knocking down Upd2 and Upd3 in ECs alleviated STAT activation in the AL (Fig.2d, Extended Data Fig.5f), and prevented the age-related decline of olfactory discrimination (Fig.2e; Extended Data Fig.5g).

This age-related decline of olfactory discrimination was independent of the microbiota, as germ-free old flies still exhibited reduced olfaction sensitivity, elevated JAK/STAT signaling in the AL, decreased numbers of EG, loss of glial cellular processes, and an enlarged AL (Extended Data Fig.6a–6d). These results are consistent with the observation that the age-related increase in Upd released from the gut is also independent of the microbiota[21].

To understand why ensheathing but not other glia selectively respond to Upd ligands and activate JAK/STAT signaling during aging or infection, we performed single-cell RNA sequencing (scRNA-seq) on purified glia from young and old flies. Either all glia (labelled using repo::Gal4) or EG selectively (labelled using GMR56F03::Gal4) were profiled using Smart-seq2 (Extended Data Fig.7a,7b). The expression of *dome* was significantly higher in

EG than in other glia (Extended Data Fig.7c), consistent with the specific upregulation of *socs36E*, a known target of JAK/STAT signaling, in ensheathing but not other glia during aging (Extended Data Fig.7d). These results are supported by a similar upregulation of *socs36E* in EG of old animals observed in a previous scRNA-seq dataset[22] (Extended Data Fig.7e, 7f).

Glial JAK reprograms lipid metabolism

Bulk RNA sequencing analysis on glia (repo::Gal4, UAS::tdTomato) purified from central brains of flies expressing a 10xSTAT::GFP reporter[16] (Extended Data Fig.7g, Supplementary Figure 1) revealed that the transcriptomes of STAT::GFP^{+} glia from *Ecc15* infected and uninfected animals were more similar to each other than to STAT::GFP^{-} glia of either condition, indicating that JAK/STAT induction has a stronger influence on glial transcriptomes than other infection-related changes (Extended Data Fig.7h). Differentially expressed genes (866 genes using a cut-off of two-fold change, p value<0.001, FDR<0.01 and reads>0.5; Extended Data Fig.7i, Supplemental Table 2), were significantly enriched in genes encoding proteins involved in lipid metabolism and carbohydrate transmembrane transport (Extended Data Fig.7j). These included the lipid binding protein glial lazarillo (Glaz, a homologue of apolipoprotein D in mammals[23]), which facilitates lipid transport from neurons to glia in flies[23], the lipid droplet surface binding proteins Lsd-1 and Lsd-2[24,25], the diacylglycerol O-acyltransferase Midway (a central regulator of triacylglycerol biosynthesis[26]), and Coatomer, which is responsible for protein delivery to lipid droplets[27] (Extended Data Fig.7k). This induction of lipid storage genes was coupled with induction of the monocarboxylate transporter (MCT) Outsiders (Out), and the MCT accessory protein Basigin (Bsg), sugar transporters (Tret1-1 and Tret1-2), and 17 enzymes involved in β-oxidation (Extended Data Fig.7l–7n).

Glial MCTs promote lipid production in neurons and lipid droplet accumulation in glia by establishing a neuron/glia “lactate shuttle”[23]. To test a potential role for STAT signaling in influencing this shuttle at the AL, we assessed lipid droplet accumulation at the AL in infected young flies using a combination of a neutral lipid probe (LipidTox, deep red) and a lipid peroxidation probe (C11-Bodipy, 581/591). We observed a transient accumulation of lipid droplets (LDs) 24 hours post infection, which decreased 4 days post infection (Extended Data Fig.8a), possibly due to elevated β-oxidation (Extended Data Fig.7m,7n)[28]. Over-expression of *Hop*^{tuml} in EG of young flies also promoted LD accumulation (Extended Data Fig.8b), while knocking down Dome or STAT rescued infection-induced LD accumulation (Extended Data Fig.8c). Glaz and Outsiders were required for LD accumulation upon infection (Extended Data Fig.8c), and over-expressing Upd2 and Upd3 in the gut induced LD accumulation at the AL, while knockdown of Upd2 or Upd3 alleviated LD accumulation in infected flies (Extended Data Fig.8d; efficiency of RNAi knockdown was confirmed by qPCR, Extended Data Fig.8e, f). Infection or JAK/STAT perturbation did not influence lipid peroxidation in LDs in young flies (Extended Data Fig.8g, 8h).

Lipotoxicity due to chronic JAK activity

During neuronal stress, neurons can preferentially transfer fatty acids to glia, causing lipid accumulation and increasing fatty acid β-oxidation in glia[28,29]. We observed a significant induction of LDs specifically in EG at the AL in old animals (Extended Data Fig.9a), phenocopying *Hop*^{tuml} over-expression (Extended Data Fig.8b). As fatty acid β-oxidation is a source of reactive oxygen species (ROS)[28,30] that can result in lipid peroxidation, and lipid peroxidation in pigment cells (glia of the retina) promotes the demise of photoreceptors in the retina[29], while oxidative stress contributes to age-related dysfunction of cholinergic projection neurons within the olfactory circuit[11], we reasoned that overall ROS levels might increase in glia with age. We expressed various genetically encoded ROS sensors in all glia (repo::Gal4) or in ensheathing glia only (GMR56F03::Gal4) to measure levels of hydrogen peroxide (H_2O_2; measured by RoGFP2_Orp1) or the glutathione redox potential (E_{GSH}; measured by RoGFP2_Grx1) within the mitochondria or cytosol, respectively. Cytosolic H_2O_2 levels were elevated in EG of old flies (both cytosolic and mitochondrial H_2O_2 levels were elevated in all glia), while cytosolic E_{GSH} remained unchanged (Extended Data Fig. 9b–9e). In contrast to acute intestinal infection in young animals, lipids were peroxidated in LDs of old animals (Extended Data Fig.9f). Knocking down STAT specifically in ensheathing glia, or knocking down Upd2 and Upd3 in gut ECs, inhibited LD accumulation and alleviated lipid peroxidation in old animals (Extended Data Fig.9f, 9g).

Olfactory discrimination was partially rescued in old and in young infected animals after Glaz and Out knockdown in EG (Fig.3a, Extended Data Fig.10a). Glaz and Out knockdown also led to more *Ecc15* food consumption, increased mortality after *PE* exposure, and reduced LD accumulation in glia of old flies (Fig.3b, 3c, Extended Data Fig.10b–10e).

To confirm that infection or aging-induced metabolic changes in EG affect neuron/glia metabolic coupling at the AL, we assessed the consequences of perturbing projection neurons (PN) directly using GH146::Gal4. Knocking down Outsiders but not lactate dehydrogenase (Ldh) in PNs rescued olfactory discrimination of infected or aged flies (Fig.3d, Extended Data Fig.10f), while food preference or mortality were not influenced (Extended Data Fig.10g, 10h). Over-expression of lipase 4 (Lip-4) in PNs, or knockdown of the neuronal lipid binding protein neural lazarillo (Nlaz), significantly improved olfactory discrimination in infected or old flies (Fig.3d, Extended Data Fig.10f), and Lip-4 over-expression increased *Ecc15* food consumption and increased mortality after PE exposure (Fig.3e, 3f, Extended Data Fig.10i).

Discussion

Our work suggest that gut-derived inflammatory cytokines modulate glia/neuron metabolic coupling in the brain of *Drosophila* to induce an adaptive temporary halt of olfactory discrimination upon intestinal infection, but also contribute to age-related olfactory decline (Fig.3g). We propose that gut-derived Upd2 and Upd3 reprogram lipid metabolism in EG, increasing lactate and lipid transport between glia and olfactory neurons, resulting in LD accumulation and upregulation of mitochondrial β-oxidation, potentially a source of elevated ROS production. Chronic activation of this metabolic shift in old animals results in the accumulation of peroxidated lipids in EG, promoting their decay and contributing to the

previously described functional decline of olfactory neurons[11]. Detailed characterization of this metabolic reprogramming, and further exploration of the role of lipid synthesis in PNs for glial lipid accumulation and for olfactory discrimination are important avenues for further study.

Our findings further elucidate the regulation of avoidance behavior against enteropathogens in insects. In addition to gustatory bitter neurons[5] and immune receptors in octopaminergic neurons[3], Upds constitute a direct endocrine signal from the damaged intestinal epithelium in this complex but essential behavior. We propose that Upd-mediated suppression of olfactory discrimination is required to prevent olfaction-mediated attraction to a food source after pathogenicity has been established and aversion is induced by gustatory neurons[5]. It remains unclear, however, whether gustatory neurons are also affected by JAK/STAT signaling in EG. Whether similar mechanisms are conserved and control infection-induced loss of sensory perception in vertebrates including humans[1,31,32] will be fascinating to explore.

Methods

Drosophila stocks and husbandry

Flies were kept on standard fly food which were prepared with the following recipe: 1L distilled water, 22g molasses, 6.26 ml propionic acid, 13.8g agar, 80g corn flour, 75g malt extract, 18g inactivated dry yeast, 10g soy flour, 2g Methyl 4-Hydroxybenzoate (MP) in 7.2 ml of EtOH. Flies were reared at the temperature indicated in corresponding figures and at 65% humidity with a 12 hour light/dark cycle, except for sterile flies and conventional control flies which were reared at room temperature with no tight control on humidity and light/dark cycle. Only female animals were used in all experiments.

The Gal4-UAS target expression system was used to conditionally express UAS-linked transgenes in the presence of indicated Gal4. Crosses with tub::$G80^{ts}$ were maintained at 18°C on standard fly food and 3 day-old female adults were transferred to 29°C to temporarily induce transgene expression, unless otherwise indicated. Crosses without tub::$G80^{ts}$ were maintained at 25°C on standard fly food.

This study follows all ethical regulations required for research using *Drosophila melanogaster* as an experimental model. Complying with NIH regulations, no ethical approval was required for work with *Drosophila melanogaster*.

The following fly lines were obtained from Bloomington *Drosophila* Stock Center: w^{1118}, Oregon-R (OreR), $Gr63a^{1}$(9941), $Orco^{1}$(23129), $mCherry^{RNAi}$(35785), UAS::Hop^{tuml}/FM7c(8492), $upd2^{RNAi}$(33988), $upd2^{RNAi}$(33949), $dome^{RNAi}$(34618), $stat^{RNAi}$(35600), ldh^{RNAi}(33640), GMR54H02Gal4(45784), GMR54C07Gal4 (50472), GMR86E01Gal4(45914), GMR56F03Gal4(39157), UAS::LacZ(1776), UAS::nls.mCherry(38425), GMR10E12Gal4(46517), SPARCGal4(77473), GMR83E12Gal4(40363), $TubG80^{ts}$(7013), 10xSTAT::GFP(26198), repoGal4(7415), UAS::lipase-4 (67142), GH146Gal4(30026), out^{RNAi} (67858),

UAS::MitoRoGFP2_Orp1(67667), nSybGal4(51635), UAS::mCD8-GFP(5137), actin::Gal4(4414), hmlGal4, UAS::2xGFP(30140), UAS::2xGFP(60292).

The following fly lines were obtained from Vienna *Drosophila* RNAi Center: *dome*^{RNAi}(106071), *stat*^{RNAi}(106980), *Glaz*^{RNAi}(15387), *Glaz*^{RNAi}(107433), *upd3*^{RNAi}(27134), *Nlaz*^{RNAi}(35558), *out*^{RNAi}(51157).

The following fly lines were gifts from other labs: 2xSTAT::GFP (Erika Bach), *LacZ*^{RNAi} (Masayuki Miura), UAS::*Hop*^{tuml}/cyo (David Bilder), *upd3*^{RNAi} (Steven Hou), UAS::upd2 (Martin Zeidler), UAS::upd3 (Nicolas Buchon), UAS::CD4GFP,UAS::RedStinger/Tm6 (Liqun Luo), NP1Gal4 (Dominique Ferrandon), Mex1Gal4;tubG80^{ts} (Lucy O'Brien), UAS::tdTomato (Michael A. Welte), cg::Gal4(Carl S. Thummel), UAS::CytoRoGFP2_Orp1 and UAS::CytoRoGFP2_Grx1 (Tobias Dick).

The genotypes, ages, and genders of flies used in each figure are detailed in Supplemental Table 1. Knockdown efficiencies of the RNAi lines used in this paper are shown in Extended Data Fig.3c, 4g, 8e and 8f.

Starvation and bacterial infection

Bacterial strains, *Ecc15* or *Pseudomonas entomophila* (*PE*), were cultured in LB medium at 29°C for 18–24 hours. Bacteria were centrifuged at 5000rpm, room temperature for 10 minutes and resuspended in 500ul 5% sucrose (OD100). Bacteria sucrose solution was then added to empty fly vials containing Whatman filter paper at the bottom. Flies were starved in empty vials for 2–3 hours before transferred to vials containing bacteria solution, except for overnight wet starvation during which flies were starved in vials containing 500ul ddH_2O on Whatman filter paper. Flies were infected with *Ecc15* for 4 hours or 24 hours as noted correspondingly, before the dissection or use in assays. To infect flies with heat-killed *Ecc15*, *Ecc15* sucrose solution was boiled at 95 °C for 30min, and cooled down before use. Mock flies were treated identically, but fed with 500ul 5% sucrose without bacteria only. For *PE* survival experiments, flies were infected in vials containing 500ul *PE* sucrose solution on Whatman filter paper continuously, and 100ul 5% sucrose was added every day to vials until the end point.

Axenic fly culture

Sterile flies were generated and aged under sterile conditions as described before[33]. In brief, embryos collected on sterile apple juice agar plates (recipe: 700ml H_2O, 22.5g Agar, 250ml apple juice, 25g sucrose, 7ml 20% Methyl 4-hydroxybenzoate in Ethanol) were bleached for 3 min in 2.7% sodium hypochlorite (2-fold diluted bleach), and washed twice with sterile ddH_2O for 1 min. To make conventional control flies, collected eggs were washed with same amount of ddH_2O instead as above. These embryos were transferred into sterile food in a tissue culture hood, followed by adding 100ul of sterile 70% glycerol on top. Flies were maintained in a laminar flow hood and flipped into new sterile food every 2–3 days. To validate axenic conditions, adult fly guts were dissected and plated onto nutrient agar plates to check commensal loads.

Immunostaining

Adult female *Drosophila* heads were dissected in 1×, PH 7.4 phosphate-buffered saline (PBS), and fixed for 20 minutes at room temperature in fixation buffer containing: 1xPBS and 4% formaldehyde. Heads were washed in washing buffer (1xPBS, 0.1% Triton X-100) for 1 hour (20min each, 3 times), followed by incubation in blocking buffer (1x PBS, 0.1% Triton X-100, 5% donkey serum) at room temperature for 1 hour. Samples were incubated in primary antibodies for two nights at 4 °C, followed by 1.5 hour washing at room temperature (30min each, 3 times), and secondary antibody incubation for 2 hours at room temperature.

Adult female *Drosophila* guts were dissected in 1×, PH 7.4 phosphate-buffered saline (PBS), and fixed for 20–30 min at room temperature in fixation buffer containing: 25 mM KCl, 100 mM glutamic acid, 1 mM MgCl2, 20 mM MgSO4, 4 mM sodium phosphate, and 4% formaldehyde. Guts were washed for 1 h at 4°C in washing buffer containing: 1× PBS, 0.5% bovine serum albumin and 0.1% Triton X-100, followed by incubation in primary antibodies overnight at 4°C, 1 h washing at 4°C, and secondary antibodies for 2 h at room temperature.

For neutral lipid droplet staining, brains were dissected and fixed as above, followed by 30min wash in washing buffer. Brains were stained with HCS LipidTOX™ Deep Red neutral lipid stain (ThermoFisher, H34477, 1:200 diluted in 1xPBS) on an orbital shake at room temperature overnight. Following one wash with 1xPBS, brains were mounted with SlowFade™ Gold Antifade Mountant (ThermoFisher, S36936) and imaged on the same day.

Primary antibodies and dilution used in this study: mouse anti-repo (DSHB 8D12, 1:100) labelling glia in the central brain[34], mouse anti-NC82 (DSHB, 1:50–1:100), rabbit anti-GFP (ClonTech, Cat# 632592, 1:500). Fluorescent secondary antibodies were bought from Jackson Immunoresearch. DAPI was used to stain DNA at 1:1000. All the images were taken on the Yokogawa CSU-W1/Zeiss 3i Marianas spinning disk confocal microscope with Hamamatsu FLASH 4.0 sCMOS camera, under 40x objective, except for live imaging (described below). All the images were processed by Adobe Illustrator 2020 and Image J.

Ex vivo live imaging of *Drosophila* brains

Adult female flies were dissected in Adult Hemolymph-like Saline (AHLS) culture media containing 2mM CaCl2, 5mM KCl, 5mM HEPES, 8.2mM MgCl2, 108mM NaCl, 4mM NaHCO3, 1mM NaH2PO4, 5mM Trehalose and 10 mM Sucrose. Brains were transferred to a 35mm glass bottom dish (MatTek, P35G-1.5–14-C), with 50–100ul 3% low melting agarose (dissolved in AHLS media) added on top. After 5 minutes, 3ml AHLS media was added in the dish, and brains were imaged on the Yokogawa CSU-W1/Zeiss 3i Marianas spinning disk confocal microscope with Photometrics Evolve EMCCD camera under 40x objective. For ratiometric CytoRoGFP2_Orp1, MitoRoGFP2_Orp1 and CytoRoGFP2_Grx1 biosensors[35], probe fluorescence was excited sequentially using the 405 nm and 488 nm laser lines and emission was detected at 500–550 nm. Imaging settings were carefully optimized prior to each experiment to ensure optimal dynamic range without saturating cameras. Identical z-stacks were acquired for each sample.

For lipid peroxidation staining and imaging, fly brains were dissected in Shields and Sang M3 insect medium (Sigma S8398) and incubated for 30 min in this medium containing LipidTox™ Deep Red (1:200) and 2 μM C11- BODIPY 581/591 (Invitrogen, D3861) at 37°C. Following two rinse with 1× PBS, brains were mounted with SlowFade™ Gold Antifade Mountant and imaged immediately with Yokogawa CSU-W1/Zeiss 3i Marianas spinning disk confocal microscope possessing Photometrics Evolve EMCCD camera, under 40x objective. Identical z-stacks were acquired for each sample. Lipid peroxidation were determined by the intensity of oxidized lipids (excitation: 488 nm, emission: 500–540 nm) over the intensity of non-oxidized lipids (excitation: 561 nm, emission: 570–610 nm).

Glia sorting, Bulk RNA sequencing and data analysis

About 100 brains were dissected for each replicate in cold Shields and Sang M3 insect medium (Sigma S8398) containing 10% fetal bovine serum (FBS; ThermoFisher,16000036). Brains were dissociated in the solution containing 300ul papain (Sigma, P4762; dissolved in 1xPBS to a final concentration of 100units/ml) and 4.1ul liberase TM solution (Roche, 5401119001; reconstituted with 1xPBS to a final centration of 2.5mg/ml) at 25°C, 1000rpm for 20min, as described before[36]. Cells were stained with Calcein blue (ThermoFisher, c1429, 1:1000) for 20min on ice, washed, and resuspended in dissection buffer with SYTOX™ Deep Red Dead cell stain (ThermoFisher, S11381, 1:1000). GFP^+ $tdTomato^+$ cells and GFP^- $tdTomato^+$ cells were sorted into Trizol (ThermoFisher, 15596026) respectively, using Fluorescence Activated Cell Sorting (FACS) with BD FACSAria™ Fusion (gating strategy is shown in Supplementary Figure 1), followed by RNA extraction. cDNA was generated from 2 nanograms of RNA using Smart-Seq V4 Ultra Low Input RNA Kit (Takara cat#: 634894). 150 picograms of cDNA was used to make sequencing libraries by Nextera XT DNA Sample Preparation Kit (Illumina cat#: FC-131–1024). Libraries were sequenced for 50 single read cycles and 30 million reads per sample on Illumina NovaSeq 6000. Reads were aligned to *Drosophila* genome (version BDGP6), using the GSNAP aligner as part of the HTSeqGenie R package (version 4.2). Reads that uniquely aligned within exonic boundaries of genes were used to derive expression estimates. nRPKM (reads per kilobase per normalized million mapped reads) where the total library sizes were normalized using the median ratio method described before[37], were generated for each gene. Differential gene expression analysis was performed in Partek Flow (Partek Inc., St Louis, MO) and Gene Ontology analysis was done using tools at Flymine.org and Geneontology.org. A list of differentially expressed genes shown in Extended Data Fig.7i is detailed in Supplemental Table 2.

Single-cell RNA sequencing using Smart-seq2 and data analysis

80–100 adult female flies at 5-or 50- day old which over-expressed mCD8::GFP specifically in glia (using repo::Gal4) or in EG (using GMR56F03::Gal4) were dissected respectively in cold Shields and Sang M3 insect medium (Sigma S8398) containing 10% fetal bovine serum (FBS; ThermoFisher,16000036). To improve glial dissociation efficiency and viability for Smart-seq2, we compared different enzyme combinations, including papain, liberase, collagenase and trypsin, and found that the combination of collagenase and trypsin performed the best. To make 1ml dissociation buffer, we mixed 250ul collagenase (2.5mg/ml, Sigma #C9891), 100ul trypsin EDTA (0.05%), and 650ul 1x PBS. Brains were

dissociated at 25°C, 1000rpm for 30min (samples were pipetted 50–100 times every 10 min). After single-cell suspension was prepared, GFP positive cells were FACs sorted into individual wells of 384-well plates using SH800 (Sony Biotechnology). Full-length poly(A)-tailed RNA was reverse-transcribed and amplified by PCR following the Smart-seq2 protocol[38]. cDNA was digested using lambda exonuclease (New England Biolabs) and then amplified for 25 cycles. Sequencing libraries were prepared from amplified cDNA, pooled, and quantified using BioAnalyser (Agilent). Sequencing was performed using the Novaseq 6000 Sequencing system (Illumina) with 100 paired-end reads and 2 × 8 bp index reads.

Reads were aligned to the *Drosophila* genome (r6.10) using STAR (2.5.4)[39]. Gene counts were produced using HTseq (0.11.2) with default settings except "-m intersection-strict"[40]. We removed low-quality cells having fewer than 10,000 uniquely mapped reads. To normalize for differences in sequencing depth across individual cells, we rescaled gene counts to counts per million reads (CPM). All analyses were performed after converting gene counts to logarithmic space via the transformation Log_2(CPM+1). For data visualization, we performed principal component analysis (PCA) on the cell x gene matrix and used tSNE to further project the top 50 PCs into a two-dimensional space. Figures were generated using scanpy in Python (version 2.7).

For data analysis in Extended Data Fig.7b, we manually curated the non-ensheathing glial population. Repo::Gal4 labels all glia, and some repo::$Gal4^+$ glial cells were clustered with ensheathing glial clusters (GMR56F03::$Gal4^+$) as expected. These cells belong to $repo^+$ ensheathing glia. We validated these cells using ensheathing glial markers. The rest repo::$Gal4^+$, GMR56F03::$Gal4^-$ cells were categorized as non-ensheathing glia. Of note, a small number of GMR56F03::$Gal4^+$ cells appeared to be non-ensheathing glia, presumably due to the non-specificity of this Gal4 driver, which were excluded from the analysis. For analysis in Extended Data Fig.7e and 7f, cells were extracted from a previously published dataset[41] in which 57k filtered brain cells that were sequenced using 10x Genomics platform.

Olfactory T-maze assay

For young flies with targeted gene over-expression or knockdown, experimental crosses were maintained at 18°C, and 3–4 day old progenies were transferred to 29°C for another 5–7 days before T-maze assay. To age flies, wild-type flies (w^{1118}xOreR) were maintained at 25°C. Experimental flies expressing $dome^{RNAi}$, $stat^{RNAi}$, $Glaz^{RNAi}$, or out^{RNAi} in the presence of GMR56F03Gal4;$tubG80^{ts}$ were aged at 25°C for 14–16 days followed by aging at 29°C for 10–14 days, unless otherwise specified. Experimental flies with $upd2^{RNAi}$ and $upd3^{RNAi}$ were aged at 29°C during the adult life for 28–30 days, while flies expressing $Nlaz^{RNAi}$, ldh^{RNAi}, out^{RNAi} and UAS::Lip-4 in PNs were aged at 25°C for 36–40 days. Axenic flies were aged at room temperature in a tissue culture hood as described above. During each experiment, a cohort of 30–90 flies were tested per condition, the result of which was considered as one replicate and was indicated as one dot in the panel.

T-maze assay was performed in the dark at 22–24°C and 35%−40% humidity. Only female flies were tested, and flies were given 1 min to make a choice before counting. Attractive

odor, Putrescine (Sigma 51799), and aversive odor, 3-Octanol (Sigma 218405) were diluted by ddH_2O and paraffin oil (Sigma 18512) respectively. 100mM Putrescine and 100mM 3-Octanol were used for wild-type flies (w^{1118} crossed with OreR), while 1M Putrescine and 10mM 3-Octanol were supplied to the rest genotypes. 50ul of odorant solution and control solution were sequentially added onto Whatman filter paper of the odorant tube and the control tube, before installed into the T-maze device. After experimentation, flies in the odorant tube and the control tube were counted. The preference index (P.I.) was calculated using the equation: P.I.=(N(odor)−N(control))/(N(odor)+N(control))*100%. Statistical analysis was performed using nonparametric Mann-Whitney test, Kruskal-Wallis test, or Dunn's multiple comparisons test in GraphPad Prism version 7.05.

CAFE assay

We modified the CAFE assay[42] by putting three flies in a transparent vial containing 1cm high 1% agar at the bottom to keep the moisture. Two 5ul capillaries were inserted into a cotton plug on top. One capillary contained liquid food, including 10% yeast, 10% sucrose, and blue dye, while the other one contained liquid food mixed with *Ecc15*. To make *Ecc15*-mixed liquid food, 40ml *Ecc15* was freshly cultured as described above, and was resuspended in 3ml liquid food. The food intakes were recorded at corresponding time points and the capillaries were changed every 24 hours.

RT-qPCR

20 guts from Np1::Gal4 flies or 10 heads from Actin::Gal4 or nSyb::Gal4 flies were collected correspondingly in Trizol (Invitrogen) per biological replicate. cDNA was synthesized using iScript™ cDNA synthesis kit (Bio-Rad). Real-time qPCR was performed on a QuantStudio 8 Flex system (ThermoFisher) with the following Taqman Probes (ThermoFisher). For data analysis, C(t) values of target genes in linear scale were normalized to actin5c.

Taqman probes: Dm01845230_g1(*outsiders*), Dm01821385_m1(*Glaz*), Dm01844576_g1(*Nlaz*), Dm01841229_g1(*Ldh*), Dm01844134_g1(*upd2*), Dm01844142_g1(*upd3*), Dm02361909_s1(*actin5c*) were used.

Intracellular flow cytometry and FACs analysis

20 brains were dissected for each biological replicate. Single cell suspension of each sample was prepared freshly, following the above dissociation step using the combination of papain and liberase. Cells was fixed, permeabilized and stained with anti-GFP antibody (ClonTech, Cat# 632592, 1:500) following a previously published protocol[43], using eBioscience™ Foxp3/Transcription Factor Staining Buffer Set (ThermoFisher Cat. No. 00–5523–00). DAPI was added to each sample at a final concentration 1 μg/mL, to stain nuclei, and analyzed by BD Symphony flow cytometer. Fluorescent secondary antibodies were bought from Jackson Immunoresearch (1:500).

FlowJo v10 Software computed the median fluorescence intensity (MFI) of GFP in $mCherry^+$ ensheathing glia, and generated histogram (x-axis: fluorescence intensity levels of channels of interest in logarithmic scale; y-axis: the number of events, noted as modal).

To overlay multiple cell populations with different sizes, the absolute cell counts were normalized to the peak height at mode of the distribution, noted as normalized to mode in y-axis.

Image quantification and statistical analyses

Images taken on live brains with CytoRoGFP2_Orp1, MitoRoGFP2_Orp1 or MitoRoGFP2_Grx1 fluorescent biosensors were analyzed with Image J. Z-stack images were converted to maximal intensity projections. For ratiometric measurements of these biosensors, the 488 nm excitation channel was used for image segmentation and ROIs detection. For CytoRoGFP2_Orp1 and CytoRoGFP2_Grx1, ROIs were carefully selected to represent each single glia at the antennal lobe manually, while automated ROI detection was optimized and utilized for MitoRoGFP2_Orp1. Mean intensity values within each ROI were calculated under 405 nm and 488 nm excitation channels sequentially. The intensity ratio of 405nm:488nm for each ROI was calculated in excel, and was compiled to generate the mean ratio for each brain sample.

To create false color ratio images, maximal intensity projections were first converted from 16 to 32-bit format. ROIs were detected manually or automatically in the same way as described above. Image background (regions outside of ROIs) was cleared. A ratio image was generated by pixel by pixel division of 405 nm image over 488 nm image. Ratio images in false color were generated in Image J using the “fire” LookUp Table (LUT).

For ratiometric measurement of lipid peroxidation in lipid droplets at the antennal lobe, maximal intensity projections were acquired from z-stack images in Image J. ROIs were manually selected to represent each neutral lipid droplet at the antennal lobe under the LipidTox Alexa 647 (deep red) channel. After applying ROIs to the 488nm (oxidized) and 561nm (non-oxidized) excitation channels, the intensity ratio of 488nm:561nm for each ROI was calculated in excel, and was compiled to generate the mean value for each brain sample. The mean value for each genotype group was normalized to the mean of control samples.

Images to be compared were collected using identical laser and detector settings. To compare protein expression level and cell numbers in fixed samples, images with same numbers of z-stacks were analyzed. Sample size and number of replicates were described in the corresponding legends. Statistical analyses were performed with Prism version 7.05 (GraphPad Software, La Jolla, CA, USA). Statistical significance was calculated using Mann-Whitney test to compare means from two independent groups, or using Kruskal-Wallis test or Dunn’s multiple comparisons test for multiple comparisons, as described in the figure legends. No statistical method was used to predetermine sample sizes. For *Ecc15* treatments, flies with the same sex, age and genotype were randomly assigned to control or experimental groups. Where cohorts of animals with defined sex, age and genotypes were compared, animals were randomly collected from breeding cages, sorted according to sex and genotype, and combined into cohorts. As all animals in a cohort were analyzed, no randomization had to be performed in the data collection.

Data and code availability

The authors declare that the data supporting the findings of this study are available within the paper and its supplementary information files. Source data are provided with this paper. Raw sequencing reads and preprocessed sequence data for Bulk RNAseq files have been deposited in GEO under accession code GSE168530. Raw scRNAseq reads and preprocessed sequence data have been deposited in GEO under accession code GSE168572. Analysis code for scRNAseq datasets is available at https://github.com/Hongjie-Li/flyglia. *Drosophila* genome (version BDGP6) is available for download at https://aug2017.archive.ensembl.org/info/data/ftp/index.html. *Drosophila* genome (r6.10) is available for download at http://ftp.flybase.net/releases/. The published scRNAseq datasets generated by Dr. Stein Aerts lab are available at https://scope.aertslab.org.

Extended Data

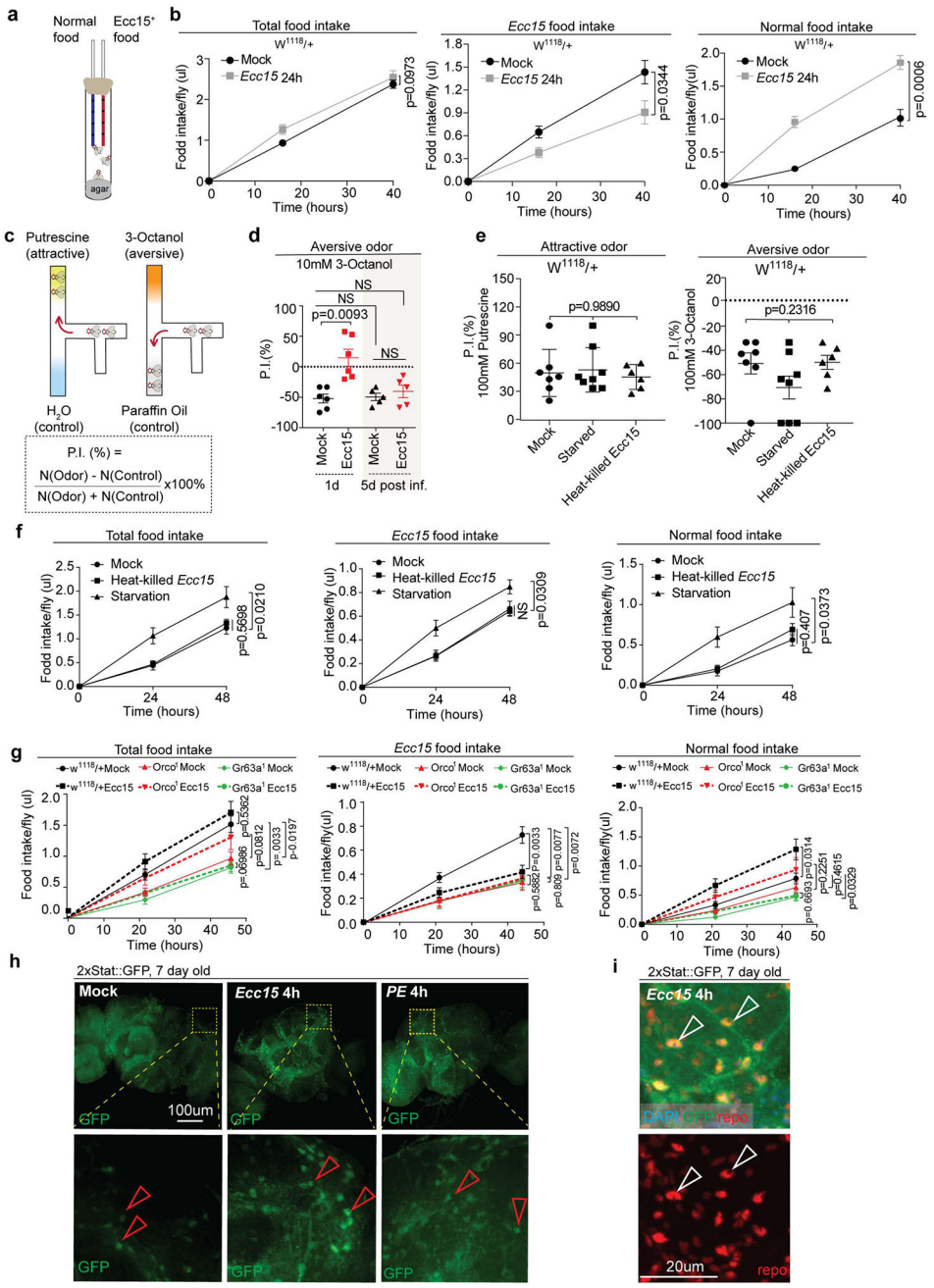

Extended Data Figure 1: Orco and Gr63 odor receptors are required for infection-induced avoidance behaviors towards enteropathogens.

(**a**) Modified CAFE assay used.

(**b**) Intake of total food, *Ecc15* containing food and normal food for wild-type flies (w^{1118}xOreR) during homeostasis and 24 hours post *Ecc15* infection respectively.

(**c**) Olfactory T-maze assay and calculation of preference index (P.I.).

(**d**) P.I. of young flies 24 hours (1d) and 5 days (5d) post *Ecc15* infection towards aversive odor, respectively.

(**e**) P.I. of wild-type flies (w^{1118}xOreR) during homeostasis, infected with heat-killed *Ecc15* or starved on water for 24 hours correspondingly.
(**f**) Intake of total food, *Ecc15* containing food and normal food for flies in **e**.
(**g**) Intake of total food, *Ecc15* containing food and normal food for wild-type flies (w^{1118}xOreR), $Gr63a^1$ flies, $Orco^1$ flies with or without *Ecc15* infection respectively.
(**h**, **i**) Representative images of 2xSTAT::GFP expression in the central brain upon 4 hour *Ecc15* infection or *PE* infection determined by immunostaining. Anti-GFP antibody amplifies 2xSTAT::GFP signal. Anti-repo immunohistochemistry to label all glia in **i**. Number quantifications of STAT+ cells per condition are shown in Fig. 1c.
Averages and s.e.m. are shown. The sample size is as follows: n=7 replicates (3 flies per cohort) per condition in **b**, **n=** n=5, 6 independently performed experiments for 1d infection and 5d post infection per respectively in **d**, **n=**7, 8, 6 independently performed experiments for mock, starved and infected flies with heat-killed *Ecc15* in **e**, n=10 replicates (3 flies per cohort) per condition in **f**, n= 7, 10, 8, 9, 10, 10 replicates (3 flies per cohort) for w^{1118} mock, w^{1118} *Ecc15*, $Orco^1$ mock, $Orco^1$ *Ecc15*, $Gr63a^1$ mock, $Gr63a^1$ *Ecc15* in **g**.
Data shown in **f**, **g** are representative of 2 independently performed experiments, and those shown in **b**, **d**, **h** and **i** are representative from 3 separate experiments. *P* values in **b**, **g** from two-tailed Mann-Whitney test; *P* values in **d**, **f** from Dunn's multiple comparisons test; other *P* values from Kruskal-Wallis test. NS=not significant (p>0.9999 in **d**, **f**).

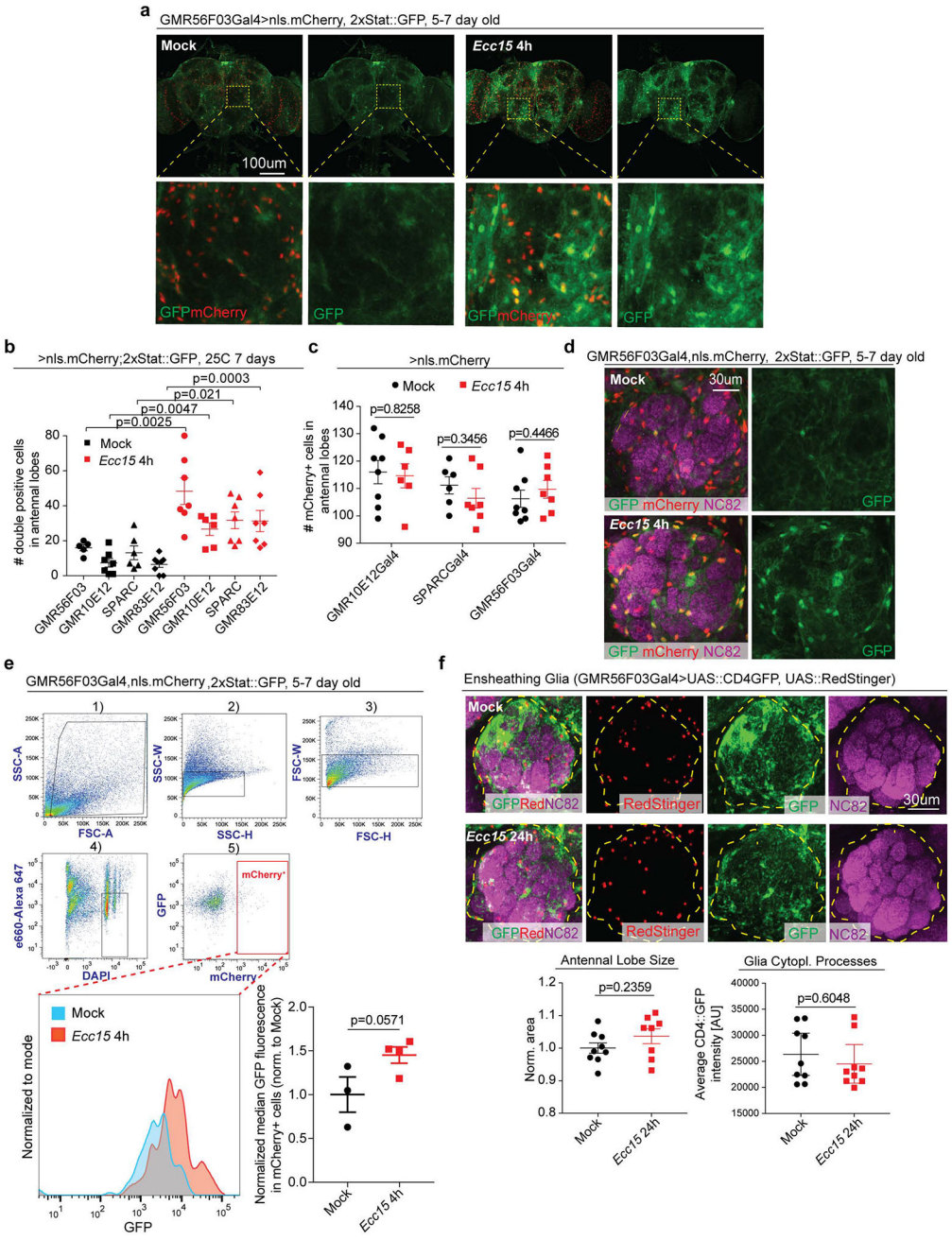

Extended Data Figure 2: Infection does not influence numbers and the morphology of ensheathing glia at the antennal lobe.

(**a**, **d**) Representative images of 2xSTAT::GFP expression in EG (nls.mCherry^{+} driven by GMR56F03::Gal4) in the central brain during homeostasis and upon 4 hour *Ecc15* infection. Antennal lobe (AL) region was zoomed in **a** and additional images were shown in **d**. Anti-GFP antibody amplifies 2xSTAT::GFP signal. Anti-NC82 antibody stained neuropils in **d**.

(**b**) Quantifications of 2xSTAT::GFP reporter activity in EG (nls.mCherry^{+} in the presence of corresponding Gal4 drivers) during homeostasis and upon *Ecc15* infection. Numbers of

GFP$^+$ mCherry$^+$ cells from both ALs were quantified from 30um z-sections (2um each). Four different EG-specific Gal4 drivers were tested correspondingly.

(**c**) Quantifications of EG numbers (nls.mCherry$^+$ driven by SPARC::Gal4, GMR10E12::Gal4 or GMR56F03::Gal4 respectively) at both ALs under mock and infected conditions.

(**e**) Histogram overlay of GFP fluorescence in mCherry $^+$ EG in the presence of GMR56F03::Gal4 under conditions as noted, measured by intracellular flow cytometry assay. X-axis: the GFP fluorescence intensity level (logarithmic scale); y-axis: the number of events (normalized to its peak height, noted as normalized to modal). Median fluorescence intensity of GFP in mCherry$^+$ EG under these conditions, was computed by FlowJo software and normalized to the median value of mock samples collected on the same day of measurement. mCherry$^+$ EG were sorted by the following gates: 1): forward versus side scatter (FSC vs SSC); 2): side scatter height versus width (SSC-H vs SSC-W); 3): forward scatter height versus width (FSC-H vs FSC-W); 4): fixable viability dye (eFluor™ 660 to label dead cells before fixation) versus DAPI (labelling nuclei to exclude debris); 5): GFP versus mCherry fluorescence channel (GFP vs mCherry).

(**f**) Representative images showing EG morphology at the antennal lobe from control and infected animals. EG Nuclei were labelled by RedStinger, while cellular processes were labelled by CD4::GFP. Anti-NC82 antibody labelled neuropils. Representative images were generated from 7 um z-sections (1um each) after performing maximal intensity projection. Average intensity levels of CD4::GFP were quantified from 20um z-stack confocal images after maximal intensity projection. AL sizes were quantified and normalized to the mean value of mock animals.

Averages and s.e.m. are shown. The sample size is as follows: n=5, 7, 6, 8, 7, 6, 7, 7 brains per condition (from left to right) in **b**, n=8, 6, 6, 7, 8, 7 brains per condition (from left to right) in **c**, n=97, 135, 822 mCherry$^+$ cells from mock flies and n=123, 91, 145, 163 mCherry$^+$ cells from infected flies in **e**, n=9, 8 brains for mock and *Ecc15* flies in **f** (left), n=9 brains per condition in **f** (right).

Data shown in **a** and **d** are representative of 3 independently performed experiments; data shown in **b**, **c**, **e**, **f** are representative of 2 independently performed experiments. *P* values in **e** from one-tailed Mann-Whitney test; other *P* values from two-tailed Mann-Whitney test.

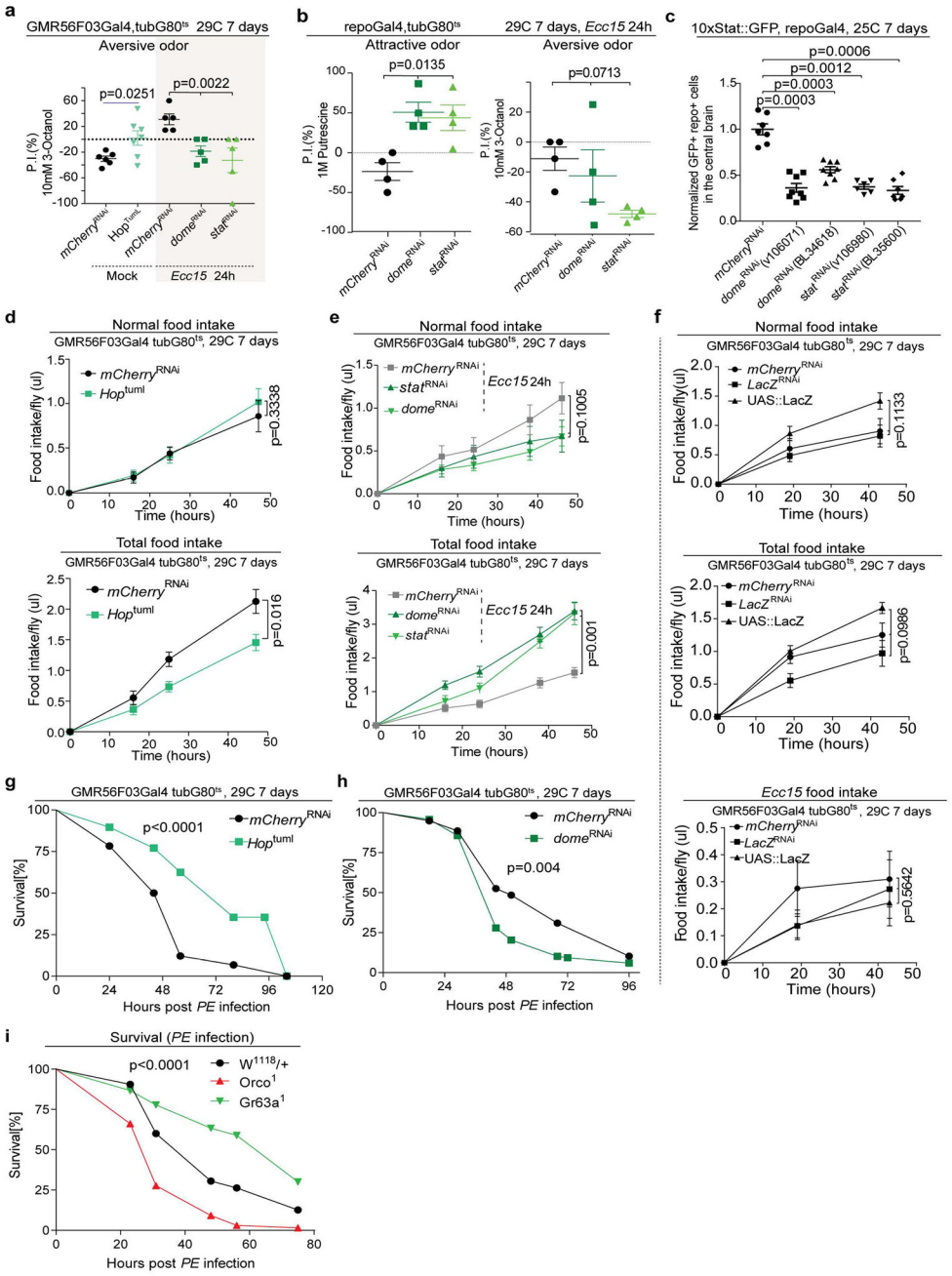

Extended Data Figure 3: JAK/STAT signaling in ensheathing glia promotes avoidance behavior against *Ecc15*, yet increasing host survival upon acute infection.

(**a**) P.I. of young flies with indicated JAK/STAT perturbation in EG. RNAi constructs were expressed in EG for 7 days by shifting animals to 29°C (restrictive temperature for Gal80^{ts}). Animals were exposed to *Ecc15* for 24 hours.

(**b**) Preference index (P.I.) of young infected flies expressing *mCherry*^{RNAi}, *Dome*^{RNAi} or *Stat*^{RNAi} in all glia (repo::Gal4;tubG80^{ts}), measured by T-maze assay.

(**c**) Quantification of STAT::GFP activity in the glia of flies knocking down *Dome*^{RNAi} or *Stat*^{RNAi} in all glia (repo::Gal4; 10xSTAT::GFP), to confirm knockdown efficiency for various RNAi lines targeting Dome or STAT correspondingly.

(**d**, **e**) Total food intake and normal food intake of flies overexpressing *Hop*^{tuml} (**d**) and of infected flies knocking down *Dome* and *Stat* (**e**) in EG (driven by GMR56F03::Gal4;tubG80^{ts}), measured by CAFE assay.

(**f**) Intake of total food, *Ecc15* containing food and normal food for flies expressing *mCherry*^{RNAi}, *LacZ*^{RNAi} and UAS::LacZ in EG during homeostasis.

(**g, h**) Survival curve of flies overexpressing *Hop*^{tuml} (**g**) or knocking down *Dome* (**h**) in EG upon continuous *PE* infection.

(**i**) Survival curves of wild-type flies (*w*^{1118}xOreR), Gr63a^{1} flies, Orco^{1} flies upon continuous *PE* infection.

Averages and s.e.m. are shown. The sample size is as follows: n=6, 7, 5, 5, 5 independently performed experiments per condition (from left to right) in **a**, n=4 independently performed experiments per condition in **b**, n=7, 8, 8, 6, 7 brains per condition (from left to right) in **c**, n=8, 9 replicates (3 flies per cohort) for *mCherry*^{RNAi} and *Hop*^{tuml} respectively in **d**, n=6, 8, 7 replicates (3 flies per cohort) for *mCherry*^{RNAi}, *Dome*^{RNAi}, *Stat*^{RNAi} in **e**, n=8 replicates per condition (3 flies per cohort) for **f**, n=74, 96 flies for *mCherry*^{RNAi} and *Hop*^{tuml} respectively for **g**, n=97, 118 flies for *mCherry*^{RNAi} and *Dome*^{RNAi} respectively for **h**, n=101, 63, 90 flies for wild-type flies (w^{1118}xOreR), Orco^{1}, Gr63a^{1} flies for **i**.

Data shown in **d**, **e**, **g**, **h** are representative of 3 independently performed experiments; data shown in **c**, **f** and **i** are representative of 2 independently performed experiments. *P* values from two-tailed Mann-Whitney test in **a** (*mCherry*^{RNAi} vs *Hop*^{tuml}), **c**, **d**; *P* values from Log-rank testin **g-i**; other *P* values from Kruskal-Wallis test.

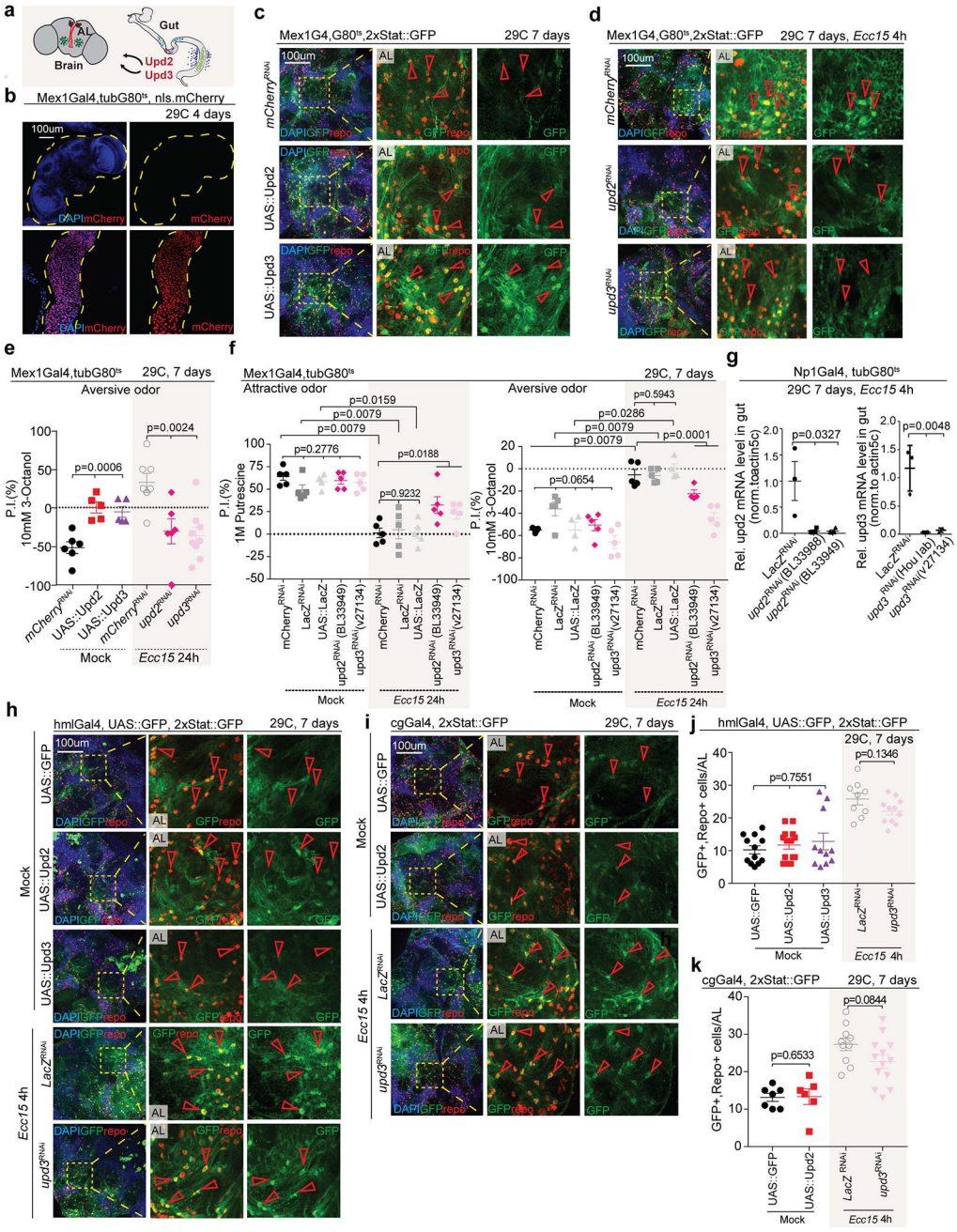

Extended Data Figure 4: Gut-derived Upd2 and Upd3 are sufficient and required for infection-induced STAT activation in the glia.

(**a**) Gut-derived Upds and their possible impact on the AL.

(**b**) Glial Expression of nuclear mCherry driven by Mex1⁚Gal4 in the gut and brain of adult flies.

(**c**, **d**) Activity of 2xSTAT⁚GFP reporter in the central brain of flies overexpressing *upd2*, *upd3* in ECs, driven by Mex1⁚Gal4;tubG80^{ts}, during homeostasis (**c**) and of infected flies loss of *upd2*, *upd3* in ECs (**d**). Representative images were generated from 30um z-sections,

and the AL region was zoomed in. Number quantifications of GFP^+, $repo^+$ glia per AL are shown in Fig. 1g.

(**e**, **f**) Preference index (P.I.) of flies expressing *mCherry*^{RNAi}, UAS::LacZ, *LacZ*^{RNAi}, UAS::upd2, UAS::upd3 and RNAi lines targeting *upd2* or *upd3* in ECs with or without *Ecc15* infection.

(**g**) qPCR analysis confirming the knockdown efficiency of multiple RNAi lines targeting *upd2* or *upd3* correspondingly.

(**h**, **j**) Activity of 2xSTAT::GFP reporter in the central brain of flies overexpressing *upd2*, *upd3* in hemocytes (driven by hm1::Gal4) during homeostasis and of infected flies loss of *upd3* in hemocytes. Numbers of GFP^+ $repo^+$ cells per AL were quantified from 30um z-sections in **j**, and the AL region was zoomed in.

(**i**, **k**) Activity of 2xSTAT::GFP reporter in the central brain of flies overexpressing *upd2* in fatbody (driven by cg::Gal4) during homeostasis and of infected flies loss of *upd3* in fatbody. Numbers of GFP^+ $repo^+$ cells per AL were quantified from 30um z-sections in **k**, and the AL region was zoomed in.

Averages and s.e.m. are shown. The sample size is as follows: n=6, 5, 5, 7, 6, 9 independently performed experiments per condition (from left to right) in **e**, n=4 or 5 independently performed experiments per condition in **f**, n=3, 4, 4 biological replicates per condition (from left to right) in **g** (left), n=3, 4, 2 biological replicates per condition (from left to right) in **g** (right), n=12, 14, 11, 9, 11 brains per condition (from left to right) in **j**, n=7, 6, 10, 13 brains per condition (from left to right) in **k**.

Data shown in **c** and **d** are representative of 3 independently performed experiments; data shown in **b**, **g**-**k** are representative of 2 independently performed experiments. *P* values from two-tailed Mann-Whitney test in **f**, **j** and **k** when comparing two groups; other *P* values from Kruskal-Wallis test.

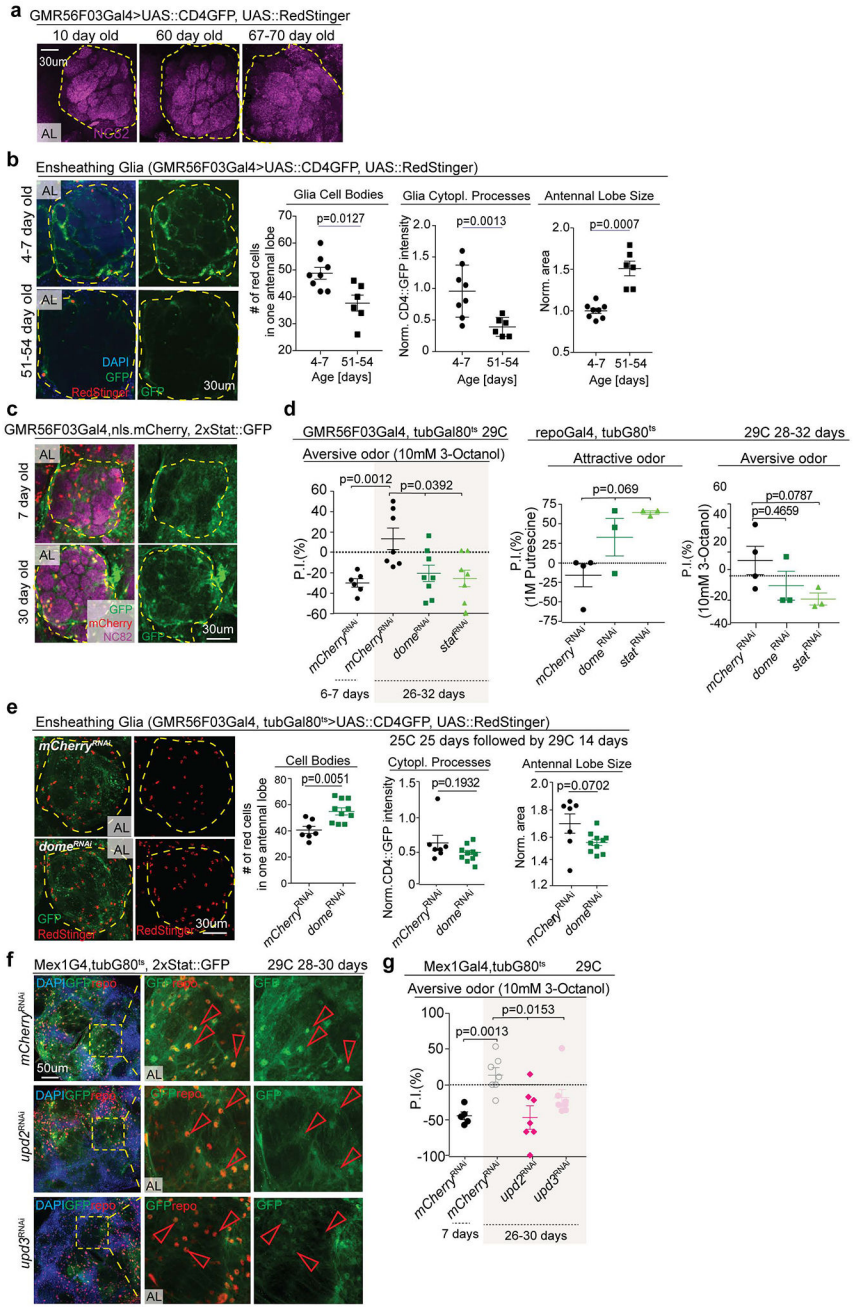

Extended Data Figure 5: Chronic activation of JAK/STAT signaling in ensheathing glia drives the decline of ensheathing glia numbers at the antennal lobe during aging.

(**a**) Representative images of glomerular compartments at the AL from young and old animals. Confocal images were generated from 20um z-sections (1um each) after performing maximal intensity projection. Anti-NC82 antibody labelled neuropils.

(**b**) Representative single z-section images showing EG morphology at the AL from young and old animals. EG nuclei were labelled by RedStinger driven by GMR56F03::Gal4, while cellular processes were labelled by CD4::GFP. Average intensity levels of CD4::GFP and AL sizes were quantified from 20um z-stack confocal images after maximal intensity projection. AL sizes were quantified and normalized to the mean values of young animals.

(**c**) Representative images of 2xSTAT::GFP reporter activity in EG (nls.mCherry^{+} driven by GMR56F03::Gal4) at the AL from young and old animals. Images were generated from 20 um z-sections (1um each) after performing maximal intensity projection.
(**d**) Preference index (P.I.) of young flies expressing *mCherry*^{RNAi} in ensheathing glia (GMR56F03::Gal4), old flies expressing *mCherry*^{RNAi}, *Dome*^{RNAi} or *Stat*^{RNAi} in ensheathing glia or all glia (repo::Gal4), measured by T-maze assay.
(**e**) Representative images showing EG morphology at the AL from old flies with or without *Dome* knockdown. EG nuclei were labelled by RedStinger in the presence of GMR56F03::Gal4;tubG80^{ts}, while cellular processes were labelled by CD4::GFP. Average intensity levels of CD4::GFP and numbers of RedStinger^{+} cells per AL were quantified. AL sizes were quantified and normalized to the mean value of old control animals. Flies were aged at 25C for 14 days followed by 29C for 14 days to induce *Dome*^{RNAi} expression.
(**f**) Representative images showing the activity of 2xSTAT::GFP reporter in the central brain of old flies knocking down *upd2* or *upd3* in ECs, driven by Mex1::Gal4;tubG80^{ts}. Representative images were generated from 30um z-sections, and the AL region was zoomed in.
(**g**) P.I. of young flies expressing *mCherry*^{RNAi} and old flies expressing *mCherry*^{RNAi}, *Upd2*^{RNAi} or *Upd3*^{RNAi} in ECs, driven by Mex1::Gal4;tubG80^{ts}.
Averages and s.e.m. are shown. The sample size is as follows: n=8, 6 brains for young and old conditions respectively in **b**, n=6, 7, 8, 7 independently performed experiments for young *mCherry*^{RNAi}, old *mCherry*^{RNAi}, *Dome*^{RNAi} and *Stat*^{RNAi} correspondingly in **d** (left), n=4, 3, 3 independently performed experiments for old *mCherry*^{RNAi}, *Dome*^{RNAi} and *Stat*^{RNAi} correspondingly in **d** (middle and right), n=7, 10 brains for *mCherry*^{RNAi}, *Dome*^{RNAi} respectively in **e**, n=5, 7, 7, 7 independently performed experiments for young *mCherry*^{RNAi}, old *mCherry*^{RNAi}, *Upd2*^{RNAi} and *Upd3*^{RNAi} correspondingly in **g**.
Data shown in **a-c**, **f** are representative of 2 independently performed experiments; data shown in **e** are representative of 3 independently performed experiments. *P* values from two-tailed Mann-Whitney test in **b**, **d** (when comparing young vs old *mCherry*^{RNAi}), **e**, **g** (when comparing young and old *mCherry*^{RNAi}); *P* values from Dunn's multiple comparisons test in **d** (right); other *P* values from Kruskal-Wallis test.

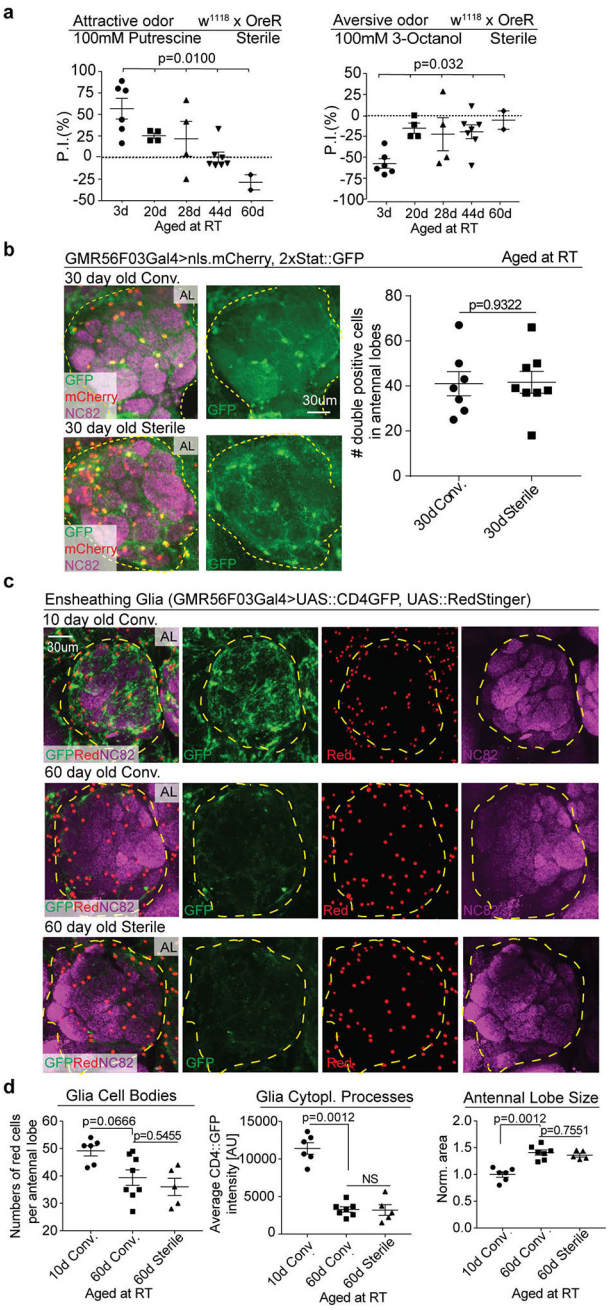

Extended Data Figure 6: Age-related decline of olfaction sensitivity and morphological decays of ensheathing glia are independent from microbiota.

(**a**) Preference index (P.I.) of germ-free wild-type flies (w^{1118}xOreR) during aging, measured by T-maze assay.

(**b**) Representative images of 2xSTAT::GFP reporter activity in EG at the AL from conventionally-reared or germ-free old flies. EG nuclei were labelled by nls.mCherry in the presence of GMR56F03::Gal4 driver. Anti-GFP antibody amplified 2xSTAT::GFP signal. Anti-NC82 antibody labelled neuropils. Confocal images were generated from 20um z-sections after performing maximal intensity projection. Flies were aged at room temperature (RT).

(**c**, **d**) Representative images showing EG morphology at the AL from young and old animals that were conventionally reared and from old germ-free animals respectively (**c**). EG nuclei were labelled by RedStinger in the presence of GMR56F03::Gal4, while cellular processes were labelled by CD4::GFP. Anti-NC82 antibody labelled neuropils. Images were generated from 20um z-sections after performing maximal intensity projection. Average intensity levels of CD4::GFP and numbers of RedStinger^{+} cells per AL were quantified in **d**. AL sizes were quantified and normalized to the mean value of young conventionally reared animals in **d**. Flies were aged at room temperature (RT).

Averages and s.e.m. are shown. The sample size is as follows: n=6, 4, 4, 7, 2 independently performed experiments per condition (from left to right) in **a**, n=7, 8 brains for 30d conventional and 30d sterile conditions respectively in **b**, n=6, 8, 5 brains per condition (from left to right) in **d** (left), n=6, 7, 5 brains per condition (from left to right) in **d** (middle and right).

Data shown in **b**-**d** are representative of 2 independently performed experiments. *P* values from Kruskal-Wallis test in **a**; other *P* values from two-tailed Mann-Whitney test.

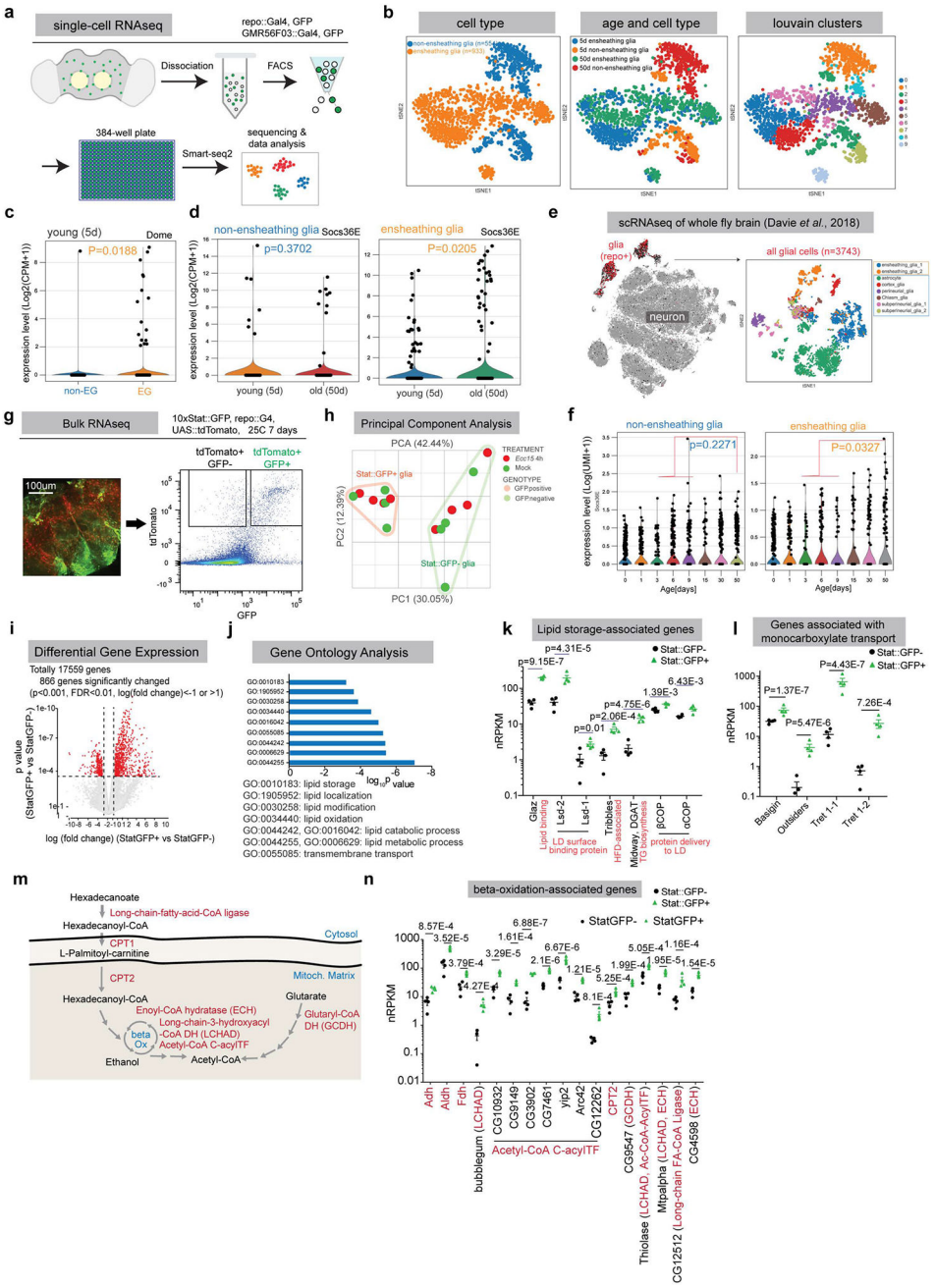

Extended Data Figure 7: JAK/STAT signaling regulates glial lipid metabolism.

(**a**) Workflow of single-cell RNA sequencing (scRNA-seq) using plate-based Smart-seq2. FACS: fluorescence-activated cell sorting. Four groups of glia were sequenced: 5d and 50d all glia (GFP$^+$, driven by rep::Gal4); 5d and 50d EG (GFP$^+$, driven by GMR56F03::Gal4). (**b**) Visualization of glial cells using tSNE plots. Cells were colored according to cell types, ages and Louvain clusters with default resolution. Non-ensheathing glia (non-EG) were curated from all repo$^+$ glia with EG (GMR56F03::Gal4$^+$) removed. See Methods. EG and non-EG were readily separated into different clusters (left and middle). In total, 10 clusters were formed from these glia (right), suggesting the heterogeneity of glial population.

(**c**) Violin plot showing expression levels of *dome* in non-EG and EG. For both EG and non-EG, cells were combined from young and old flies. In non-EG, *dome* expression was barely detected except in one cell. In EG, a subset of cells showed high expression of *dome*.
(**d**) Violin plots showing expression levels of *Socs36E* in young and old non-EG (left) and EG (right) respectively.
(**e**) Visualization of all annotated glial cells from a previously published whole fly brain scRNA-seq dataset (Davie *et al*. 2018) using tSNE plot. scRNA-seq was performed using droplet-based 10x Genomics platform. Glia were colored in red (repo^{+}), while neurons were colored in grey. Two subsets of EG (in orange box) and six subsets of non-EG (in blue box) were annotated.
(**f**) Violin plots showing expression levels of *socs36E* in non-EG and EG at eight different ages. Cells from 3 day-, 6 day- and 9 day-old flies were combined as young samples, and were compared with cells from 50 day-old flies (old).
(**g**) Gating strategy for sorting STAT::GFP^{+} glia and STAT::GFP^{-} glia from the central brain of young mock or young infected (4 hour *Ecc15* infection) flies overexpressing tdTomato in all glia (repo::Gal4) while expressing 10xSTAT::GFP reporter.
(**h**) Visualization of gene expression variation between STAT::GFP^{+} glia and STAT::GFP^{-} glia by PCA plot. Each dot represents a sample replicate independently collected from a cohort of 100 flies. Samples with the same genotype were grouped together, while samples with different treatments were colored separately.
(**i**) Volcano plot displaying differentially expressed genes between STAT::GFP^{+} glia and STAT::GFP^{-} glia (highlighted in red) under homeostatic conditions, using a cut-off of two-fold change, p value<0.001, FDR<0.01.
(**j**) Gene Ontology analysis of significantly upregulated genes in STAT::GFP^{+} glia during homeostasis.
(**k**) Lipid storage-associated genes were significantly upregulated in STAT::GFP^{+} glia during homeostasis. nRPKM values of each gene in STAT::GFP^{+} glia and STAT::GFP^{-} glia were shown correspondingly.
(**l**) Genes involved in monocarboxylate transport were significantly upregulated in STAT::GFP^{+} glia during homeostasis. nRPKM values of each gene in STAT::GFP^{+} glia and STAT::GFP^{-} glia were shown correspondingly.
(**m**) Schematic demonstrating mitochondrial fatty acid β-oxidation.
(**n**) Genes involved in fatty acid β-oxidation that were significantly upregulated in STAT::GFP^{+} glia during homeostasis. nRPKM values of each gene in STAT::GFP^{+} glia and STAT::GFP^{-} glia were shown correspondingly.
Averages and s.e.m. are shown. The sample size is as follows: n=4 replicates per condition (each replicate was independently pooled from 100 flies on different days) in **g**-**n**. *P* values in **k**, **l** and **n** were calculated by Partek Flow; *P* values in **c**, **d** and **f** from one-tailed Student's t-test.

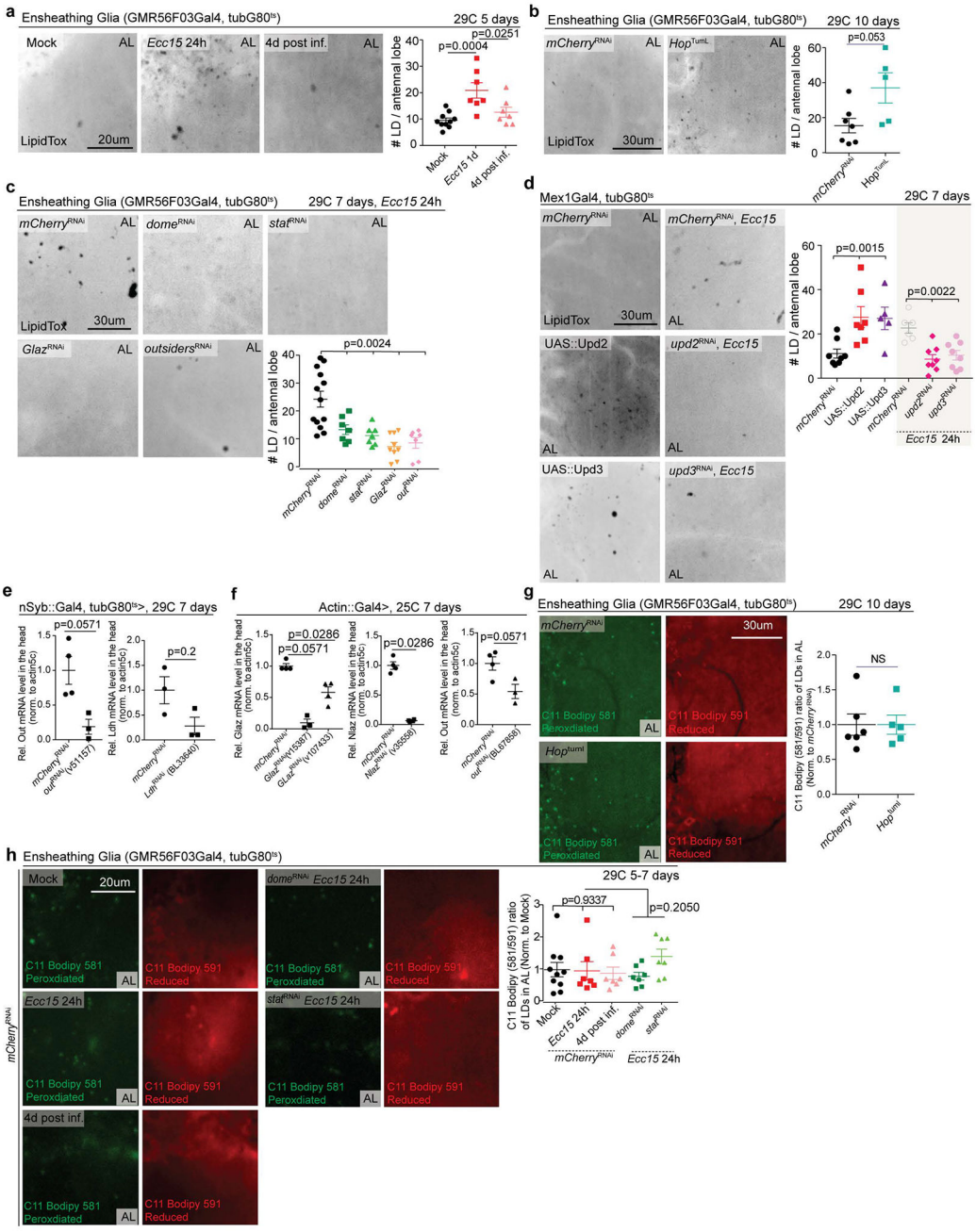

Extended Data Figure 8: JAK/STAT signaling regulates LD accumulation via *Glaz* and *Outsiders* upon infection, with no influence on lipid peroxidation.

(**a**) Immunostaining detecting lipid droplets (LDs) at the AL from young flies during homeostasis, 24 hours post *Ecc15* infection, or 4 days post infection, using LipidTox deep red probes. LD numbers per AL were quantified.

(**b**, **c**) Immunostaining detecting LDs at the AL from young flies overexpressing *mCherry*^{RNAi} or *Hop*^{tuml} in EG (driven by GMR56F03::Gal4;tubG80^{ts}) during homeostasis (**b**), and from infected flies knocking down *Dome*, *Stat*, *Glaz* or *Outsiders* in EG (**c**). LD numbers per AL were quantified.

(**d**) Immunostaining detecting LDs at the AL from young flies overexpressing Upd cytokines in ECs, driven by Mex1::Gal4;tubG80^{ts}, during homeostasis, and from infected flies knocking down Upd cytokines in ECs. LD numbers per antennal lobe were quantified.
(**e**, **f**) qPCR analysis confirming the knockdown efficiency of multiple RNAi lines targeting *Out*, *Glaz*, *Nlaz*, *and Ldh* respectively.
(**g**, **h**) Representative images showing lipid peroxidation in LDs at the AL from young flies expressing *mCherry*^{RNAi} or *Hop*^{tuml} in EG (driven by GMR56F03::Gal4;tubG80^{ts}) during homeostasis (**g**), from young mock flies, infected flies or 4 days post *Ecc15* infection (**h**), and from infected flies knocking down *Dome* or *Stat* in EG (**h**). Lipid peroxidation levels of LDs for each sample were measured as the mean intensity ratios of 488nm:561nm in LDs. The ratios were normalized to the mean value of corresponding control samples.
Averages and s.e.m. are shown. The sample size is as follows: n=10, 7, 7 brains per condition (from left to right) in **a**, n=7, 5 brains for *mCherry*^{RNAi}, *Hop*^{tuml} respectively in **b**, n=13, 7, 7, 9, 7 brains per condition for *mCherry*^{RNAi}, *Dome*^{RNAi}, *Stat*^{RNAi}, *Glaz*^{RNAi}, *Out*^{RNAi} in **c**, n=8, 7, 5, 6, 8, 8 brains per condition (from left to right) in **d**, n=4 and 3 biological replicates for *mCherry*^{RNAi}, *Out*^{RNAi} in **e** (left), n=3 biological replicates for *mCherry*^{RNAi}, *Ldh*^{RNAi} in **e** (right), n=4, 3, 4, 4, 4, 4, 3 biological replicates per condition (from left to right) in **f**, n=6 and 5 brains *mCherry*^{RNAi} and *Hop*^{tuml} in **g**, n=10, 7, 7, 7, 7 brains per condition (from left to right) in **h**.
Images shown in **a-e, h-i** were generated from 20um z-sections (1um each) after performing maximal intensity projection. Data shown in **a-d, g-h** are representative of 3 independently performed experiments; data shown in **e** and **f** are representative of 2 separate experiments. *P* values in **a**, **b**, **e, f** and **g** from two-tailed Mann-Whitney test; other *P* values from Kruskal-Wallis test. NS=not significant (*P*>0.9999 in **g**).

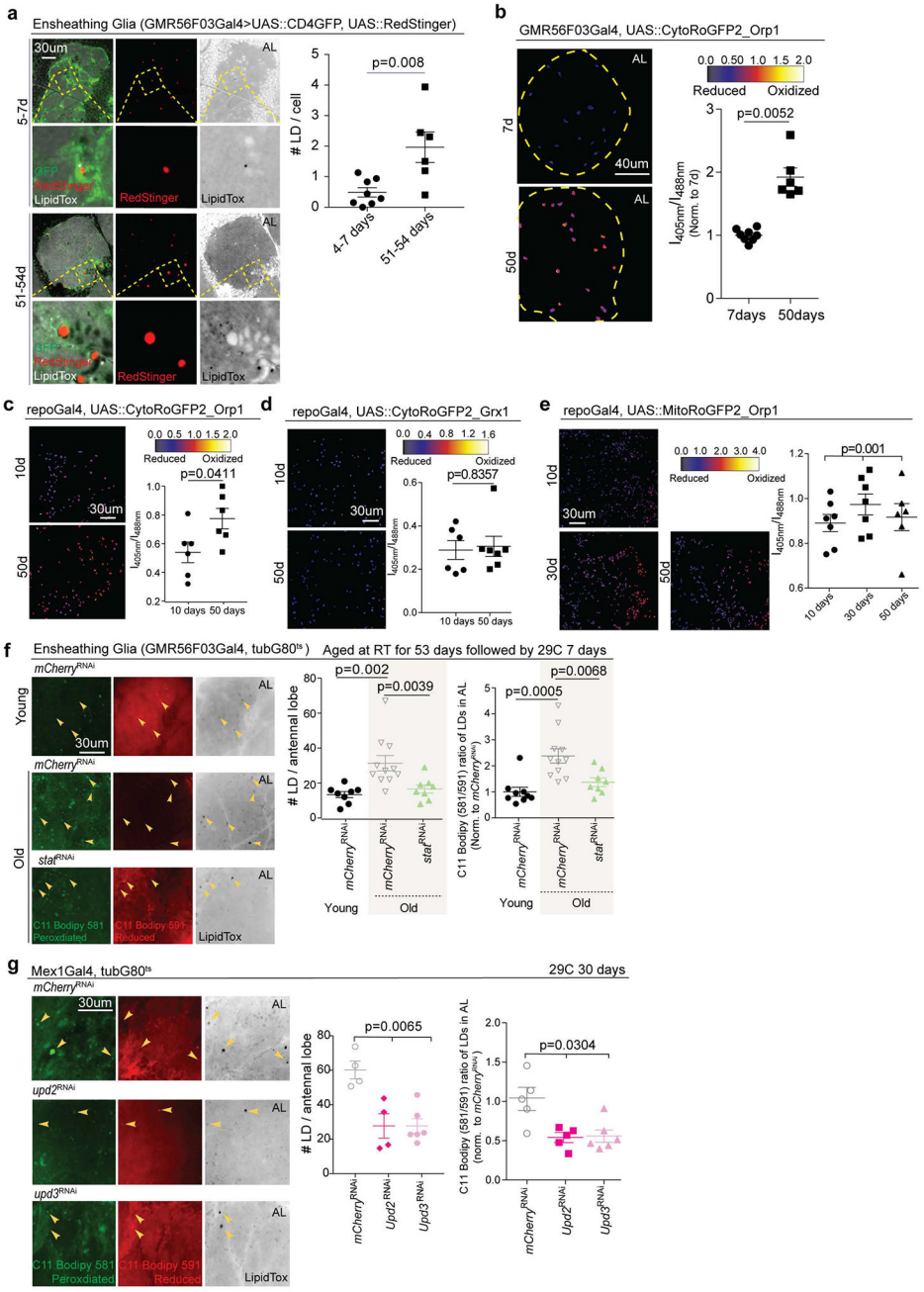

Extended Data Figure 9: Deactivation of JAK/STAT signaling alleviates lipid toxicity during aging, thus rescuing the age-related decline of ensheathing glia numbers.

(**a**) Immunostaining detecting LDs in EG (RedStinger^{+}, CD4::GFP^{+}) at the AL of young (5–7 day old) and old (51–54 day old) animals, using LipidTox deep red probes. LD numbers per glia were quantified.

(**b**) Cytosolic H_2O_2 levels in EG at the AL from young (7 day old) and old (50 day old) animals, measured as the mean intensity ratio of 405nm:488nm. The ratios for old animals were normalized to the mean value for young animals.

(**c**-**e**) Levels of cytosolic H_2O_2 (**c**), cytosolic glutathione redox potential (**d**) and mitochondrial H_2O_2 (**e**) in all glia (driven by repo::Gal4) from young and old animals, measured as the mean intensity ratios of 405nm:488nm for corresponding ROS sensors.
(**f**) Representative images showing lipid peroxidation in LDs at the AL from young flies expressing *mCherry*^{RNAi} in EG (driven by GMR56F03::Gal4;tubG80^{ts}) and from old flies expressing *mCherry*^{RNAi} or *Stat*^{RNAi} in EG. LD numbers per AL were quantified. Lipid peroxidation levels of LDs for each sample were measured as the mean intensity ratio of 488nm:561nm. The ratios were normalized to the mean value of young control samples. Flies were aged at room temperature (RT) before transferred to 29C for 7 days.
(**g**) Representative images showing lipid peroxidation in LDs at the AL from old flies loss of *upd2* or *upd3* in ECs driven by Mex1::Gal4;tubG80^{ts}. LD numbers per AL were quantified. Lipid peroxidation levels of LDs for each sample were measured as the mean intensity ratio of 488nm:561nm. The ratios were normalized to the mean value of old control samples. Averages and s.e.m. are shown. The sample size is as follows: n=8 and 6 brains for young and old conditions correspondingly in **a**, **b**, n=6 brains per condition in **c**, n=6 and 7 brains for young and old conditions correspondingly in **d**, n=7, 7, 6 brains per condition (from left to right) in **e**, n=8, 11, 8 brains per condition (from left to right) correspondingly in **f** (left), n=9, 11, 8 brains per condition (from left to right) correspondingly in **f** (right), n=4, 4, 6 brains per condition (from left to right) in **g** (left), n=5, 5, 6 brains per condition (from left to right) in **g** (right).
Images shown in **a**-**g** were generated from 20um z-sections (1um each) after performing maximal intensity projection. Data shown in **a**-**e** are representative of 2 independently performed experiments, and those shown in **f** and **g** are representative of 3 separate experiments. *P* values in **a**-**d**, **f** from two-tailed Mann-Whitney test; other *P* values from Kruskal-Wallis test.

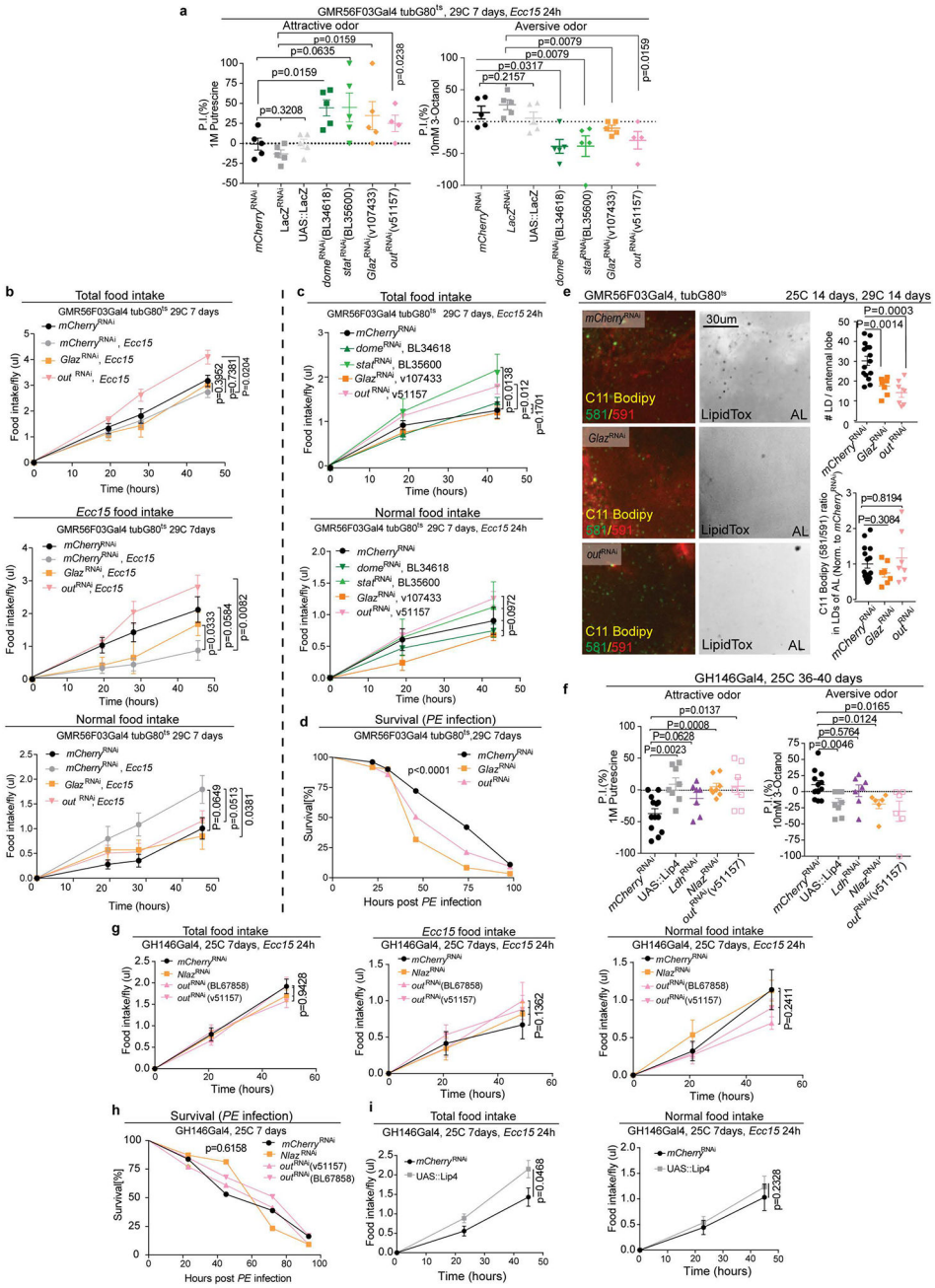

Extended Data Figure 10: Inhibiting lipid export or lactate intake in projection neurons partially rescues the decline of olfaction sensitivity upon infection and during aging.

(**a**) Preference index (P.I.) of young infected flies knocking down *Dome*, *Stat*, *Glaz* or *Outsiders* (*out*) in EG with additional RNAi lines.

(**b, c**) Intake of total food, *Ecc15*$^{+}$ food and normal food for mock flies during homeostasis and for infected flies loss of *Dome*, *Stat*, *Glaz* or *Out*, measured by CAFE assay. *Glaz*$^{\text{RNAi}}$ and *Out*$^{\text{RNAi}}$ lines in **b** and **c** are different.

(**d**) Survival curve of young flies loss of *Glaz* or *Out* upon continuous *PE* infection. *Glaz*$^{\text{RNAi}}$ and *Out*$^{\text{RNAi}}$ lines are the same as flies in **b**.

(**e**) Representative images showing LD accumulation and lipid peroxidation at the AL from old flies with knockdown of *Glaz* or *Out* in EG driven by GMR56F03::Gal4;tubG80^{ts}. LD numbers per AL were quantified. Lipid peroxidation levels of LDs for each sample were measured as the mean intensity ratio of 488nm:561nm. The ratios were normalized to the mean value of old control samples. Flies were aged at 25C for 14 days followed by 29C 14 days to induce expression of RNAi lines.

(**f**) P.I. values of old flies overexpressing Lip-4, or knocking down *Nlaz*, *Ldh*, or *Out* in projection neurons (PNs) using GH146::Gal4 driver.

(**g**) Intake of total food, *Ecc15*$^{+}$ food and normal food for young infected flies knocking down *Nlaz*, or *Out* in PNs.

(**h**) Survival curve of flies knocking down *Nlaz* or *Out* in PNs upon continuous *PE* infection.

(**i**) Intake of total food and normal food for young infected flies over-expressing Lip-4 in PNs. Averages and s.e.m. are shown. The sample size is as follows: n=5, 5, 5, 5, 5, 5, 4 independently performed experiments per condition (from left to right) in **a**, n= 6, 6, 5, 7 replicates (3 flies per cohort) for mock *mCherry*^{RNAi}, *Ecc15 mCherry*^{RNAi}, *Ecc15 Glaz*^{RNAi}, *Ecc15 Out*^{RNAi} correspondingly in **b**, n= 8, 8, 8, 7, 6 replicates (3 flies per cohort) for *mCherry*^{RNAi}, *Dome*^{RNAi}, *Stat*^{RNAi}, *Glaz*^{RNAi}, *Out*^{RNAi} correspondingly in **c**, n=100, 59, 85 flies for *mCherry*^{RNAi}, *Glaz*^{RNAi}, *Out*^{RNAi} respectively in **d**, n=15, 7, 7 brains per condition (from left to right) in **e**, n=13, 8, 7, 8, 7 independently performed experiments per condition (from left to right) in **f**, n= 6, 7, 8, 7 replicates for *mCherry*^{RNAi}, *Nlaz*^{RNAi}, *Out*^{RNAi}(v51157), *Out*^{RNAi}(BL67858) correspondingly in **g**, n=49, 86, 87, 53 flies for *mCherry*^{RNAi}, *Nlaz*^{RNAi}, *Out*^{RNAi}(v51157), *Out*^{RNAi}(BL67858), respectively in **h**, n=8 replicates (3 flies per cohort) per condition in **i**.

Data shown in **b-d, g, h** are representative of 2 independently performed experiments, and those shown in **e** and **i** are representative from 3 separate experiments. *P* values in **d** and **h** from Log-rank test; *P* values in **a** (when comparing *mCherry*^{RNAi}, *LacZ*^{RNAi} and UAS::LacZ), **c** (top: when comparing *mCherry*^{RNAi}, *Dome*^{RNAi} and *Glaz*^{RNAi}; bottom) and **g** from Kruskal-Wallis test; other *P* values from two-tailed Mann-Whitney test.

Supplementary Material

Refer to Web version on PubMed Central for supplementary material.

Acknowledgement

We thank Drs. Erika Bach, David Bilder, Steven Hou, Martin Zeidler, Nicolas Buchon, Dominique Ferrandon, Lucy O'Brien, Michael A. Welte, Masayuki Miura, Carl S. Thummel and Tobias Dick for flies. We thank Dr. Meredith Sagolla for the training in Yokogawa CSU-W1/Zeiss 3i Marianas spinning disk confocal microscope, the Genentech NGS technology core lab for the support with Bulk RNA-seq, Dr. Ilona C Grunwald Kadow for the tips in olfactory T-maze assay.

Funding

National Institutes of Health (R01AG057353) and Genentech, Inc

- Heinrich Jasper

National Institutes of Health (R00AG062746)

- Hongjie Li

National Institutes of Health (K99AG056680)

- Martin B Jensen

National Institutes of Health (R56AG057304)

- Pejmun Haghighi

National Institutes of Health (R01DC005982)

- Liqun Luo

Howard Hughes Medical Institute (Investigator)

- Liqun Luo

Chan Zuckerberg Biohub (Investigator)

- Stephen R Quake

Cancer Prevention & Research Institute of Texas (Scholar)

- Hongjie Li

The funders had no role in study design, data collection and interpretation, or the decision to submit the work for publication.

References

1. Wang A et al. Opposing Effects of Fasting Metabolism on Tissue Tolerance in Bacterial and Viral Inflammation. Cell 166, 1512–1525.e1512, doi:10.1016/j.cell.2016.07.026 (2016). [PubMed: 27610573]
2. Ayres JS & Schneider DS The role of anorexia in resistance and tolerance to infections in Drosophila. PLoS Biol 7, e1000150, doi:10.1371/journal.pbio.1000150 (2009). [PubMed: 19597539]
3. Kobler JM, Rodriguez Jimenez FJ, Petcu I & Grunwald Kadow IC Immune Receptor Signaling and the Mushroom Body Mediate Post-ingestion Pathogen Avoidance. Curr Biol, doi:10.1016/j.cub.2020.09.022 (2020).
4. Stensmyr MC et al. A conserved dedicated olfactory circuit for detecting harmful microbes in Drosophila. Cell 151, 1345–1357, doi:10.1016/j.cell.2012.09.046 (2012). [PubMed: 23217715]
5. Charroux B, Daian F & Royet J Drosophila Aversive Behavior toward Erwinia carotovora carotovora Is Mediated by Bitter Neurons and Leukokinin. iScience 23, 101152, doi:10.1016/j.isci.2020.101152 (2020). [PubMed: 32450516]
6. Soria-Gomez E, Bellocchio L & Marsicano G New insights on food intake control by olfactory processes: the emerging role of the endocannabinoid system. Mol Cell Endocrinol 397, 59–66, doi:10.1016/j.mce.2014.09.023 (2014). [PubMed: 25261796]
7. Soria-Gómez E et al. The endocannabinoid system controls food intake via olfactory processes. Nature Neuroscience 17, 407–415, doi:10.1038/nn.3647 (2014). [PubMed: 24509429]
8. Liang L & Luo L The olfactory circuit of the fruit fly Drosophila melanogaster. Sci China Life Sci 53, 472–484, doi:10.1007/s11427-010-0099-z (2010). [PubMed: 20596914]
9. Liu H et al. Astrocyte-like glial cells physiologically regulate olfactory processing through the modification of ORN-PN synaptic strength in Drosophila. Eur J Neurosci 40, 2744–2754, doi:10.1111/ejn.12646 (2014). [PubMed: 24964821]
10. Wu B, Li J, Chou YH, Luginbuhl D & Luo L Fibroblast growth factor signaling instructs ensheathing glia wrapping of Drosophila olfactory glomeruli. Proc Natl Acad Sci U S A 114, 7505–7512, doi:10.1073/pnas.1706533114 (2017). [PubMed: 28674010]
11. Hussain A et al. Inhibition of oxidative stress in cholinergic projection neurons fully rescues aging-associated olfactory circuit degeneration in Drosophila. Elife 7, doi:10.7554/eLife.32018 (2018).
12. Wu SC, Cao ZS, Chang KM & Juang JL Intestinal microbial dysbiosis aggravates the progression of Alzheimer's disease in Drosophila. Nat Commun 8, 24, doi:10.1038/s41467-017-00040-6 (2017). [PubMed: 28634323]

13. Keshavarzian A, Engen P, Bonvegna S & Cilia R The gut microbiome in Parkinson's disease: A culprit or a bystander? Prog Brain Res 252, 357–450, doi:10.1016/bs.pbr.2020.01.004 (2020). [PubMed: 32247371]
14. Jiang H et al. Cytokine/Jak/Stat signaling mediates regeneration and homeostasis in the Drosophila midgut. Cell 137, 1343–1355, doi:10.1016/j.cell.2009.05.014 (2009). [PubMed: 19563763]
15. Tracy Cai X et al. AWD regulates timed activation of BMP signaling in intestinal stem cells to maintain tissue homeostasis. Nat Commun 10, 2988, doi:10.1038/s41467-019-10926-2 (2019). [PubMed: 31278345]
16. Bach EA et al. GFP reporters detect the activation of the Drosophila JAK/STAT pathway in vivo. Gene Expr Patterns 7, 323–331, doi:10.1016/j.modgep.2006.08.003 (2007). [PubMed: 17008134]
17. Freeman MR Drosophila Central Nervous System Glia. Cold Spring Harb Perspect Biol 7, doi:10.1101/cshperspect.a020552 (2015).
18. Chakrabarti S et al. Remote Control of Intestinal Stem Cell Activity by Haemocytes in Drosophila. PLoS Genet 12, e1006089, doi:10.1371/journal.pgen.1006089 (2016). [PubMed: 27231872]
19. Rajan A & Perrimon N Drosophila cytokine unpaired 2 regulates physiological homeostasis by remotely controlling insulin secretion. Cell 151, 123–137, doi:10.1016/j.cell.2012.08.019 (2012). [PubMed: 23021220]
20. Doty RL & Kamath V The influences of age on olfaction: a review. Front Psychol 5, 20, doi:10.3389/fpsyg.2014.00020 (2014). [PubMed: 24570664]
21. Li H, Qi Y & Jasper H Preventing Age-Related Decline of Gut Compartmentalization Limits Microbiota Dysbiosis and Extends Lifespan. Cell Host Microbe 19, 240–253, doi:10.1016/j.chom.2016.01.008 (2016). [PubMed: 26867182]
22. Davie K et al. A Single-Cell Transcriptome Atlas of the Aging Drosophila Brain. Cell 174, 982–998.e920, doi:10.1016/j.cell.2018.05.057 (2018). [PubMed: 29909982]
23. Liu L, MacKenzie KR, Putluri N, Maletic-Savatic M & Bellen HJ The Glia-Neuron Lactate Shuttle and Elevated ROS Promote Lipid Synthesis in Neurons and Lipid Droplet Accumulation in Glia via APOE/D. Cell Metab 26, 719–737.e716, doi:10.1016/j.cmet.2017.08.024 (2017). [PubMed: 28965825]
24. Fauny JD, Silber J & Zider A Drosophila Lipid Storage Droplet 2 gene (Lsd-2) is expressed and controls lipid storage in wing imaginal discs. Dev Dyn 232, 725–732, doi:10.1002/dvdy.20277 (2005). [PubMed: 15704138]
25. Men TT, Binh TD, Yamaguchi M, Huy NT & Kamei K Function of Lipid Storage Droplet 1 (Lsd1) in Wing Development of Drosophila melanogaster. Int J Mol Sci 17, doi:10.3390/ijms17050648 (2016).
26. Kühnlein RP Thematic review series: Lipid droplet synthesis and metabolism: from yeast to man. Lipid droplet-based storage fat metabolism in Drosophila. J Lipid Res 53, 1430–1436, doi:10.1194/jlr.R024299 (2012). [PubMed: 22566574]
27. Soni KG et al. Coatomer-dependent protein delivery to lipid droplets. J Cell Sci 122, 1834–1841, doi:10.1242/jcs.045849 (2009). [PubMed: 19461073]
28. Ioannou MS et al. Neuron-Astrocyte Metabolic Coupling Protects against Activity-Induced Fatty Acid Toxicity. Cell 177, 1522–1535.e1514, doi:10.1016/j.cell.2019.04.001 (2019). [PubMed: 31130380]
29. Liu L et al. Glial lipid droplets and ROS induced by mitochondrial defects promote neurodegeneration. Cell 160, 177–190, doi:10.1016/j.cell.2014.12.019 (2015). [PubMed: 25594180]
30. Rosca MG et al. Oxidation of fatty acids is the source of increased mitochondrial reactive oxygen species production in kidney cortical tubules in early diabetes. Diabetes 61, 2074–2083, doi:10.2337/db11-1437 (2012). [PubMed: 22586586]
31. Brann DH et al. Non-neuronal expression of SARS-CoV-2 entry genes in the olfactory system suggests mechanisms underlying COVID-19-associated anosmia. Sci Adv 6, doi:10.1126/sciadv.abc5801 (2020).
32. Salmon Ceron D et al. Self-reported loss of smell without nasal obstruction to identify COVID-19. The multicenter Coranosmia cohort study. J Infect 81, 614–620, doi:10.1016/j.jinf.2020.07.005 (2020). [PubMed: 32650110]

33. Li H, Qi Y & Jasper H Preventing Age-Related Decline of Gut Compartmentalization Limits Microbiota Dysbiosis and Extends Lifespan. Cell Host Microbe 19, 240–253, doi:10.1016/j.chom.2016.01.008 (2016). [PubMed: 26867182]
34. Hakim-Mishnaevski K, Flint-Brodsly N, Shklyar B, Levy-Adam F & Kurant E Glial Phagocytic Receptors Promote Neuronal Loss in Adult Drosophila Brain. Cell Rep 29, 1438–1448.e1433, doi:10.1016/j.celrep.2019.09.086 (2019). [PubMed: 31693886]
35. lbrecht SC, Barata AG, Grosshans J, Teleman AA & Dick TP In vivo mapping of hydrogen peroxide and oxidized glutathione reveals chemical and regional specificity of redox homeostasis. Cell Metab 14, 819–829, doi:10.1016/j.cmet.2011.10.010 (2011). [PubMed: 22100409]
36. Li H et al. Classifying Drosophila Olfactory Projection Neuron Subtypes by Single-Cell RNA Sequencing. Cell 171, 1206–1220.e1222, doi:10.1016/j.cell.2017.10.019 (2017). [PubMed: 29149607]
37. Anders S & Huber W Differential expression analysis for sequence count data. Genome Biol 11, R106, doi:10.1186/gb-2010-11-10-r106 (2010). [PubMed: 20979621]
38. Picelli S et al. Full-length RNA-seq from single cells using Smart-seq2. Nat Protoc 9, 171–181, doi:10.1038/nprot.2014.006 (2014). [PubMed: 24385147]
39. Dobin A et al. STAR: ultrafast universal RNA-seq aligner. Bioinformatics 29, 15–21, doi:10.1093/bioinformatics/bts635 (2013). [PubMed: 23104886]
40. Anders S, Pyl PT & Huber W HTSeq--a Python framework to work with high-throughput sequencing data. Bioinformatics 31, 166–169, doi:10.1093/bioinformatics/btu638 (2015). [PubMed: 25260700]
41. Davie K et al. A Single-Cell Transcriptome Atlas of the Aging Drosophila Brain. Cell 174, 982–998.e920, doi:10.1016/j.cell.2018.05.057 (2018). [PubMed: 29909982]
42. Ja WW et al. Prandiology of *Drosophila* and the CAFE assay. Proceedings of the National Academy of Sciences 104, 8253–8256, doi:10.1073/pnas.0702726104 (2007).
43. Tracy Cai X et al. AWD regulates timed activation of BMP signaling in intestinal stem cells to maintain tissue homeostasis. Nat Commun 10, 2988, doi:10.1038/s41467-019-10926-2 (2019). [PubMed: 31278345]

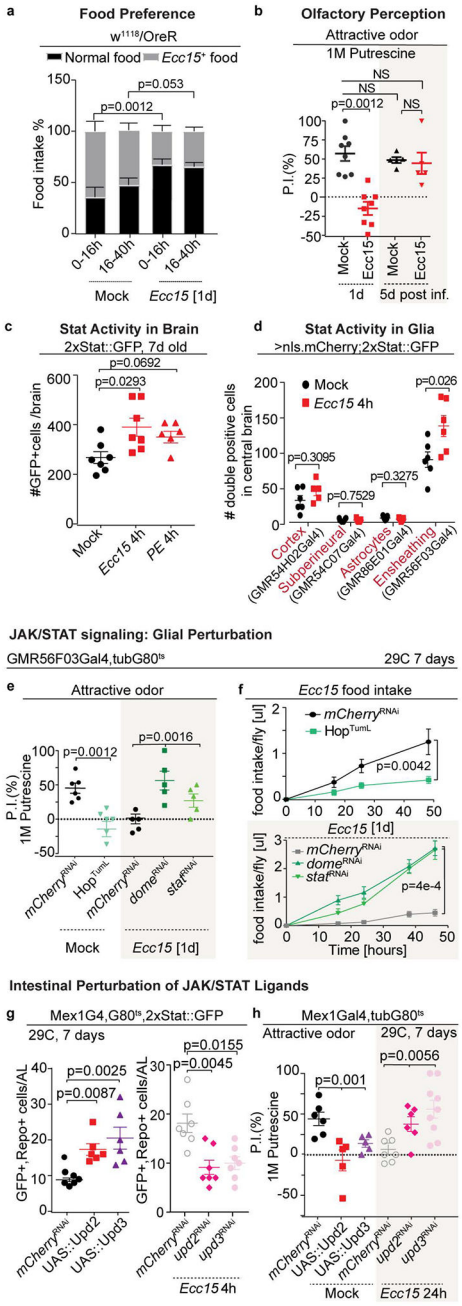

Figure 1: JAK/STAT signaling in EG upon infection transiently inhibits olfactory discrimination, contributing to *Ecc15* aversion, and host survival.

(**a**) Percentages of normal food intake and of *Ecc15*$^{+}$ food intake for wild-type flies with or without *Ecc15* infection.

(**b**) P.I. towards Putrescine of young flies 24 hours (1d) and 5 days (5d) post *Ecc15* infection.

(**c**) Numbers of STAT::GFP^{+} cells in the central brains from flies infected or not with *Ecc15* or *PE* for 4 hours. 48um z-sections were quantified per condition. Images are shown in Extended Data Fig.1h.

(**d**) STAT activity in each subtype of glia with or without *Ecc15* infection.

(**e**) P.I. towards Putrescine of young flies with indicated JAK/STAT perturbation in EG.

(**f**) Intake of *Ecc15*$^{+}$ food by young flies with indicated JAK/STAT perturbation in EG.
(**g**) Numbers of STAT::GFP^{+} glia per AL from young flies with indicated *upd2* or *upd3* perturbation in ECs. Images are shown in Extended Data Fig. 4c, 4d.
(**h**) P.I. towards Putrescine of young flies with indicated perturbations of *upd2* or *upd3* in ECs. Averages and s.e.m. are shown. n=7 replicates (3 flies per cohort) per condition in **a**, n=8, 8, 5, 5 independently performed experiments per condition (from left to right) in **b**, n=7, 7, 6 brains per condition (from left to right) in **c**, n=6, 5, 6, 7, 7, 7, 6, 6 brains per condition (from left to right) in **d**, n=6, 7, 5, 5, 5 independently performed experiments per condition (from left to right) in **e**, n= 8, 9 replicates (3 flies per cohort) for *mCherry*^{RNAi}, *Hop*^{tuml} in **f** (top), 6, 8, 7 replicates for *mCherry*^{RNAi}, *Dome*^{RNAi}, *Stat*^{RNAi} in **f** (bottom). n=7, 6, 6 flies for *mCherry*^{RNAi}, UAS::Upd2 and UAS::Upd3 in **g** (left), n=7 flies per condition in **g** (right), n=6, 5, 5, 7, 6, 9 independently performed experiments per condition (from left to right) in **h**.
Data shown in **d** are representative of 2 independently performed experiments, and those shown in **a**, **c**, **f**, **g** are representative from 3 separate experiments. *P* values in **a**, **d**, **e** (left) and **f** (top) from two-tailed Mann-Whitney test; *P* values in **b**, **c**, **g** from Dunn's multiple comparisons test; other *P* values from Kruskal-Wallis test. NS=not significant (p>0.9999 in **b**).

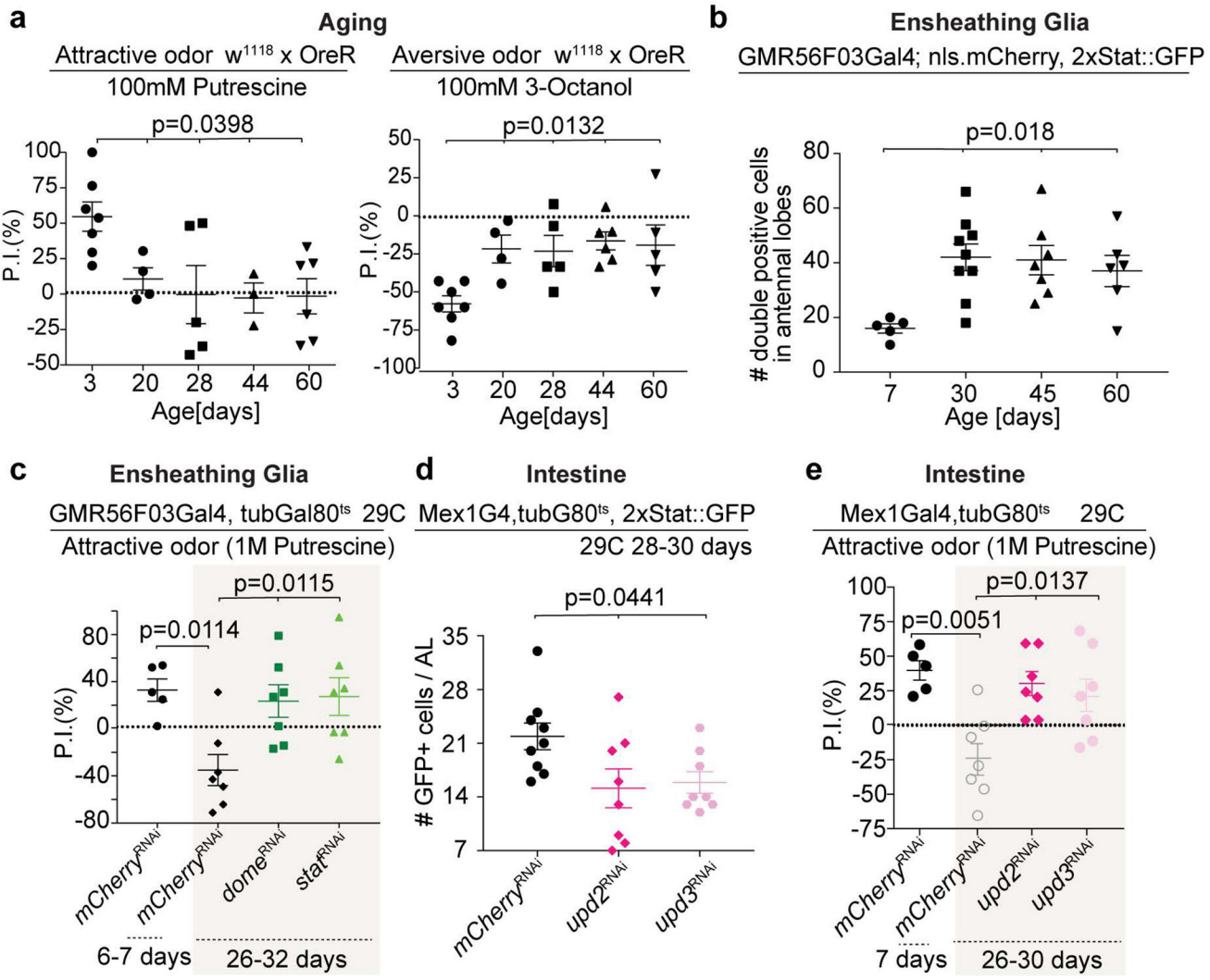

Figure 2: Chronic activation of JAK/STAT signaling in old EGs causes decline of olfaction sensitivity during aging.

(**a**) P.I. of young and old wild-type (w^{1118} x OreR) flies.

(**b**) 2xSTAT::GFP expression in EG at the AL during aging. Images are shown in Extended Data Fig.5c.

(**c**) P.I. of young control flies and of old flies with indicated perturbations in EG.

(**d**) Numbers of 2xSTAT::GFP^{+} glia per AL of old flies with indicated perturbation in ECs. Images are shown in Extended Data Fig.5f.

(**e**) P.I. of young control flies and of old flies with indicated perturbations in ECs.

Averages and s.e.m. are shown. n=7, 4, 5, 3, 6 independently performed experiments per condition (from left to right) in **a**, n=5, 9, 7, 6 brains per condition (from left to right) in **b**, n=5, 7, 7, 7 independently performed experiments per condition (from left to right) in **c**, n= n=9, 8, 8 brains per condition (from left to right) in **d**, n=5, 7, 7, 7 independently performed experiments per condition (from left to right) in **e**.

Data shown in **b** and **d** are representative of 2 independently performed experiments. *P* values from two-tailed Mann-Whitney test in **c** and **e** when comparing young and old *mCherry*^{RNAi}; other *P* values from Kruskal-Wallis test.

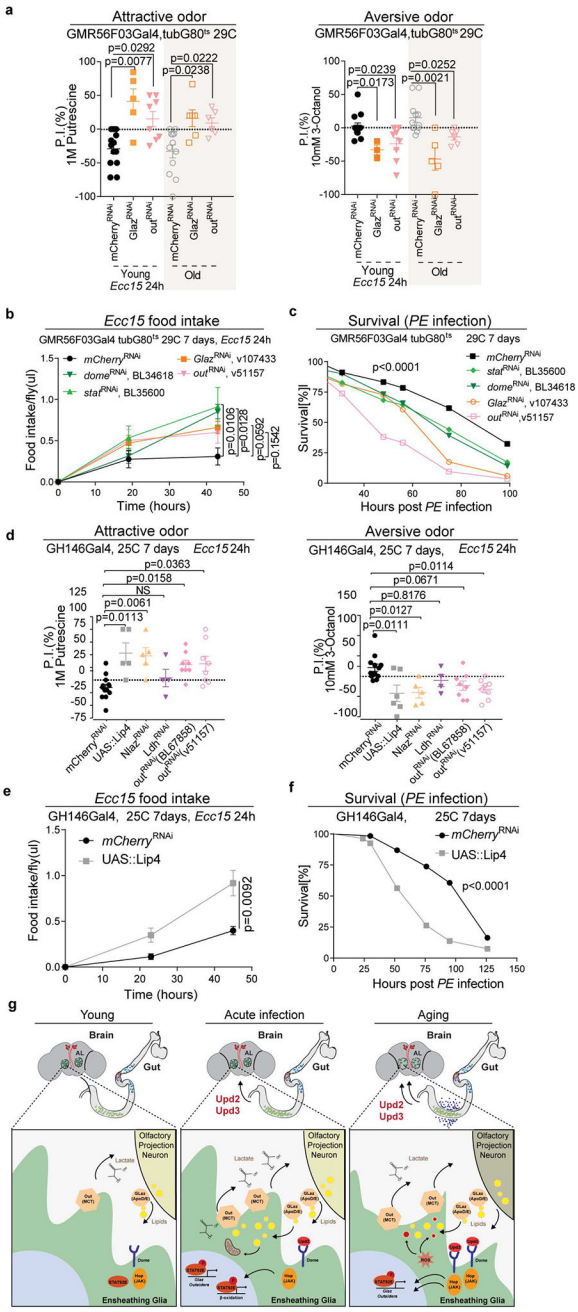

Figure 3: Disrupting the glia/neuron lactate shuttle in the AL aggravates infection-caused mortality, yet partially alleviates age-related olfactory degeneration.

(**a**) P.I. of young infected flies and of old flies after knockdown of the indicated genes in EG.

(**b**) *Ecc15*$^{+}$ food intake of young infected flies after knockdown of the indicated genes in EG.

(**c**) Survival curve of young flies upon continuous *PE* infection after knockdown of the indicated genes in EG.

(**d**) P.I. of young infected flies with indicated perturbation in PNs.

(**e**) *Ecc15*$^{+}$ food intake of young infected flies overexpressing Lip-4 in PNs.

(**f**) Survival curve of flies overexpressing Lip-4 upon continuous *PE* infection.

(**a-f**) Averages and s.e.m. are shown. n=13, 5, 8, 12, 6, 6 independently performed experiments per condition(from left to right) in **a** (left), n=14, 3, 8, 12, 5, 6 independently performed experiments per condition(from left to right) in **a** (right), n= 8, 8, 8, 7, 6 replicates (3 flies per cohort) per condition for *mCherry*^{RNAi}, *Dome*^{RNAi}, *Stat*^{RNAi}, *Glaz*^{RNAi} and *Out*^{RNAi} respectively in **b**, n=102, 120, 104, 132 and 84 flies for *mCherry*^{RNAi}, *Dome*^{RNAi}, *Stat*^{RNAi}, *Glaz*^{RNAi} and *Out*^{RNAi} respectively in **c**, n=13, 5, 5, 4, 8, 8 independently performed experiments per condition (from left to right) in **d** (left), n=13, 6, 5, 4, 8, 8 independently performed experiments per condition (from left to right) in **d** (right), n=8 replicates (3 flies per cohort) per condition in **e**, n=61 and 80 flies for *mCherry*^{RNAi} and Lip-4 correspondingly in **f**.

Data shown in **b**, **c** are representative of 2 independently performed experiments, and those shown in **e**, **f** are representative from 3 separate experiments. *P* values from two-tailed Mann-Whitney test in **e**; *P* values in **c** and **f** from Log-rank test; other *P* values from Dunn's multiple comparisons test. NS=not significant ($P>0.9999$ in **d**).

(**g**) Model for the impact of gut-derived cytokines on neuron/glia metabolic coupling at the antennal lobe.